



U.S. Department of  
Transportation

Federal Railroad  
Administration

## Impact Test Data Analysis for Load Environment Characterization of Tank Car Stub Sill During Yard Operations

---

Office of Research,  
Development  
and Technology  
Washington, DC 20590



#### NOTICE

This document is disseminated under the sponsorship of the Department of Transportation in the interest of information exchange. The United States Government assumes no liability for its contents or use thereof. Any opinions, findings and conclusions, or recommendations expressed in this material do not necessarily reflect the views or policies of the United States Government, nor does mention of trade names, commercial products, or organizations imply endorsement by the United States Government. The United States Government assumes no liability for the content or use of the material contained in this document.

#### NOTICE

The United States Government does not endorse products or manufacturers. Trade or manufacturers' names appear herein solely because they are considered essential to the objective of this report.

<b>REPORT DOCUMENTATION PAGE</b>			<i>Form Approved</i> <i>OMB No. 0704-0188</i>	
Public reporting burden for this collection of information is estimated to average 1 hour per response, including the time for reviewing instructions, searching existing data sources, gathering and maintaining the data needed, and completing and reviewing the collection of information. Send comments regarding this burden estimate or any other aspect of this collection of information, including suggestions for reducing this burden, to Washington Headquarters Services, Directorate for Information Operations and Reports, 1215 Jefferson Davis Highway, Suite 1204, Arlington, VA 22202-4302, and to the Office of Management and Budget, Paperwork Reduction Project (0704-0188), Washington, DC 20503.				
1. AGENCY USE ONLY (Leave blank)		2. REPORT DATE March 2020		3. REPORT TYPE AND DATES COVERED Technical Report
4. TITLE AND SUBTITLE Impact Test Data Analysis for Load Environment Characterization of Tank Car Stub Sill During Yard Operations			5. FUNDING NUMBERS 693JJ6-18-F-000117	
6. AUTHOR(S) Sajjad Meymand, Ph.D.				
7. PERFORMING ORGANIZATION NAME(S) AND ADDRESS(ES) ENSCO, Inc 5400 Port Royal Rd Springfield, VA 22151			8. PERFORMING ORGANIZATION REPORT NUMBER SERV-REPT-0002336	
9. SPONSORING/MONITORING AGENCY NAME(S) AND ADDRESS(ES) U.S. Department of Transportation Federal Railroad Administration Office of Railroad Policy and Development Office of Research, Development and Technology Washington, DC 20590			10. SPONSORING/MONITORING AGENCY REPORT NUMBER DOT/FRA/ORD-20/09	
11. SUPPLEMENTARY NOTES COR: Francisco González, III				
12a. DISTRIBUTION/AVAILABILITY STATEMENT This document is available to the public through the FRA <a href="#">website</a> .			12b. DISTRIBUTION CODE	
13. ABSTRACT (Maximum 200 words) Fractures in the stub sills of tank cars pose a significant problem for the rail industry due to the potential for damage to the tank structure and eventual release of the contents. Previous research by the Federal Railroad Administration (FRA) revealed that high magnitude coupling forces that occur in yard operations have the potential to exceed yield limits of mild steel. In 2018, FRA, Union Tank Car, and Amsted Rail completed a cooperative test program at Amsted Rail's test facility in Camp Hill, PA, to characterize coupling loads for tank cars in yard operations. FRA contracted ENSCO, Inc. to conduct more than 700 impact tests simulating various coupling conditions. For each impact test, 40 data channels comprised of acceleration, force, speed, and strain were recorded. The test data was analyzed to study the effect of different parameters on the coupling behavior. The statistical analysis revealed that the peak longitudinal coupler force is mostly influenced by coupling speed and draft gear type, not configurations of loaded and empty cars. However, the impulse at the impact, a measure of transferred energy between cars, is largely dependent on configurations of loaded and empty cars as opposed to draft gear type.				
14. SUBJECT TERMS Tank cars, rail, stub sill failures, impact test, yard operation, car coupling, draft gear, instrumented couplers, hazardous materials			15. NUMBER OF PAGES 47	
			16. PRICE CODE	
17. SECURITY CLASSIFICATION OF REPORT Unclassified	18. SECURITY CLASSIFICATION OF THIS PAGE Unclassified	19. SECURITY CLASSIFICATION OF ABSTRACT Unclassified	20. LIMITATION OF ABSTRACT	

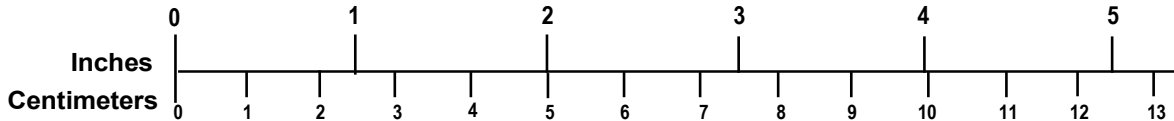
# METRIC/ENGLISH CONVERSION FACTORS

## ENGLISH TO METRIC

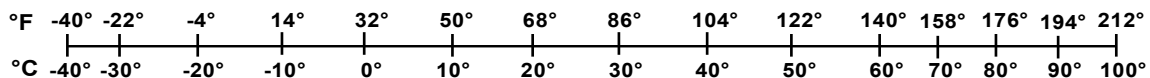
## METRIC TO ENGLISH

<p style="text-align: center;"><b>LENGTH (APPROXIMATE)</b></p> <p>1 inch (in) = 2.5 centimeters (cm)                      1 foot (ft) = 30 centimeters (cm)                      1 yard (yd) = 0.9 meter (m)                      1 mile (mi) = 1.6 kilometers (km)</p>	<p style="text-align: center;"><b>LENGTH (APPROXIMATE)</b></p> <p>1 millimeter (mm) = 0.04 inch (in)                      1 centimeter (cm) = 0.4 inch (in)                      1 meter (m) = 3.3 feet (ft)                      1 meter (m) = 1.1 yards (yd)                      1 kilometer (km) = 0.6 mile (mi)</p>
<p style="text-align: center;"><b>AREA (APPROXIMATE)</b></p> <p>1 square inch (sq in, in<sup>2</sup>) = 6.5 square centimeters (cm<sup>2</sup>)                      1 square foot (sq ft, ft<sup>2</sup>) = 0.09 square meter (m<sup>2</sup>)                      1 square yard (sq yd, yd<sup>2</sup>) = 0.8 square meter (m<sup>2</sup>)                      1 square mile (sq mi, mi<sup>2</sup>) = 2.6 square kilometers (km<sup>2</sup>)                      1 acre = 0.4 hectare (he) = 4,000 square meters (m<sup>2</sup>)</p>	<p style="text-align: center;"><b>AREA (APPROXIMATE)</b></p> <p>1 square centimeter (cm<sup>2</sup>) = 0.16 square inch (sq in, in<sup>2</sup>)                      1 square meter (m<sup>2</sup>) = 1.2 square yards (sq yd, yd<sup>2</sup>)                      1 square kilometer (km<sup>2</sup>) = 0.4 square mile (sq mi, mi<sup>2</sup>)                      10,000 square meters (m<sup>2</sup>) = 1 hectare (ha) = 2.5 acres</p>
<p style="text-align: center;"><b>MASS - WEIGHT (APPROXIMATE)</b></p> <p>1 ounce (oz) = 28 grams (gm)                      1 pound (lb) = 0.45 kilogram (kg)                      1 short ton = 2,000 pounds (lb) = 0.9 tonne (t)</p>	<p style="text-align: center;"><b>MASS - WEIGHT (APPROXIMATE)</b></p> <p>1 gram (gm) = 0.036 ounce (oz)                      1 kilogram (kg) = 2.2 pounds (lb)                      1 tonne (t) = 1,000 kilograms (kg) = 1.1 short tons</p>
<p style="text-align: center;"><b>VOLUME (APPROXIMATE)</b></p> <p>1 teaspoon (tsp) = 5 milliliters (ml)                      1 tablespoon (tbsp) = 15 milliliters (ml)                      1 fluid ounce (fl oz) = 30 milliliters (ml)                      1 cup (c) = 0.24 liter (l)                      1 pint (pt) = 0.47 liter (l)                      1 quart (qt) = 0.96 liter (l)                      1 gallon (gal) = 3.8 liters (l)                      1 cubic foot (cu ft, ft<sup>3</sup>) = 0.03 cubic meter (m<sup>3</sup>)                      1 cubic yard (cu yd, yd<sup>3</sup>) = 0.76 cubic meter (m<sup>3</sup>)</p>	<p style="text-align: center;"><b>VOLUME (APPROXIMATE)</b></p> <p>1 milliliter (ml) = 0.03 fluid ounce (fl oz)                      1 liter (l) = 2.1 pints (pt)                      1 liter (l) = 1.06 quarts (qt)                      1 liter (l) = 0.26 gallon (gal)                      1 cubic meter (m<sup>3</sup>) = 36 cubic feet (cu ft, ft<sup>3</sup>)                      1 cubic meter (m<sup>3</sup>) = 1.3 cubic yards (cu yd, yd<sup>3</sup>)</p>
<p style="text-align: center;"><b>TEMPERATURE (EXACT)</b></p> <p style="text-align: center;">[(x-32)(5/9)] °F = y °C</p>	<p style="text-align: center;"><b>TEMPERATURE (EXACT)</b></p> <p style="text-align: center;">[(9/5) y + 32] °C = x °F</p>

### QUICK INCH - CENTIMETER LENGTH CONVERSION



### QUICK FAHRENHEIT - CELSIUS TEMPERATURE CONVERSION



For more exact and or other conversion factors, see NIST Miscellaneous Publication 286, Units of Weights and Measures. Price \$2.50 SD Catalog No. C13 10286

Updated 6/17/98

## **Acknowledgements**

---

This research team of Amsted Rail, Union Tank Car, and ENSCO, Inc. were brought together under the leadership of the Federal Railroad Administration's (FRA) Office of Research, Development and Technology Program Manager Mr. Francisco González, III, as well as FRA's Office of Railroad Safety Mr. Adam Konrad for his support and technical guidance throughout this study. This study would not be possible without the generosity of Amsted Rail and its staff, Mr. John Deppen and Mr. Andrew Seidel, for providing access to the test track and logistics for conducting the tests. A special note of gratitude is extended to Mr. Robert Toms of Union Tank Car for his technical guidance and also for facilitating the donation of the tank car to FRA and the industry as a research tool for tank car studies.

# Contents

---

Executive Summary .....	1
1. Introduction.....	2
1.1 Background .....	2
1.2 Objectives.....	4
1.3 Overall Approach .....	4
1.4 Scope .....	5
1.5 Organization of the Report .....	5
2. Test Methodology .....	6
2.1 Instrumented Tank Car .....	6
2.2 Impact Test Program .....	14
2.3 Test Matrix and Data Collected.....	15
2.4 Issues Encountered During Testing.....	17
3. Impact Test Data Analysis and Results .....	18
3.1 Filtering Data.....	18
3.2 Secondary Impact .....	20
3.3 Force Data Analysis .....	21
3.4 Strain Gage Data Analysis .....	27
3.5 Acceleration Data Analysis .....	31
3.6 Impact Force versus Impulse.....	32
3.7 Impulse Data Analysis.....	33
4. Conclusion .....	36
5. References.....	37
Abbreviations and Acronyms .....	38

## Illustrations

---

Figure 1. Stub Sill Fracture Observed in Callahan, FL, from December 2009 (Sundaram, 2014) .	2
Figure 2. Stub Sill Fracture Observed in Charleston, WV, from January 2010 (Sundaram, 2014)	3
Figure 3. Instrumented Tank Car	3
Figure 4. Detail View of the Stub Sill and Head Brace Attached to the Tank of the Instrumented Tank Car.	4
Figure 5. Schematic Diagram of Tank Car’s Instrumentation	6
Figure 6. Instrumented Coupler for Measuring Longitudinal Coupler Forces	6
Figure 7. Shear Strain Gages Installed on the Stub Sill for Measuring Vertical Coupler Force ...	7
Figure 8. Shoulder Pad Strain Gage Installed Above the Head Shoe at the A-End of the Instrumented Tank Car	8
Figure 9. In-Board Strain Gage Installed Under the Car at the End of the Stub Sill Beam.	8
Figure 10. Strain Gage Installed on the Head Shoe Close to the Corner	8
Figure 11. Strain Gage Installed on the Stub Sill Close to the Rear Stop.	9
Figure 12. Strain Gage Installed on Top of the Stub Sill Close to the Head Shoe	9
Figure 13. Tri-Axial Accelerometer Mounted on Top of the Carbody.	10
Figure 14. Dual-Axis Accelerometer Mounted on the Stub Sill on Each End of the Car	10
Figure 15. Junction Box with Data Collection System Hardware	11
Figure 16. Solar Panel and Battery Box on Top of the Instrumented Tank Car	11
Figure 17. Vertical Coupler Force Calibration Setup	13
Figure 18. Vertical Coupler Force Calibration Results	13
Figure 19. Instrumented Tank Car at the Amsted Test Track.	15
Figure 20. Draft Gears Used During Impact Test Program	17
Figure 21. Sample Longitudinal Coupler Force with Different Low Pass Filters in Time Domain	19
Figure 22. Impact Signal and Noise Floor Frequency Contents with Different Low Pass Filters	19
Figure 23. Median Filtering Used for Removing Invalid Spikes in the Speed Signal.	20
Figure 24. Arrangement of Test Cars Resulting in Secondary Impacts with Multiple Hammer Cars	20
Figure 25. Coupling Force versus Coupling Speed for Secondary Impacts	21

Figure 26. Coupling Force versus Coupling Speed Plots for Different Coupling Conditions During the Impact Test Program.....	22
Figure 27. Impact Force Data Comparison for Different Hammer Configurations and Anvil Configurations with One and Three Hopper Cars .....	23
Figure 28. Impact Force Data Comparison for Different Anvil Configurations Using Full and Empty Tank Cars as Hammer .....	23
Figure 29. Impact Force Data Comparison for Different End-of-Car Units for a Given Hammer and Anvil Configurations Using Full Tank Car and Full Tank Car Plus Three Hopper Cars .....	24
Figure 30. Impact Force Data Comparisons for Different End-of-Car Units .....	24
Figure 31. Coupler Force versus Speed for All Impact Tests.....	25
Figure 32. Comparison of Struck and Non-Struck End Impact Force for Different Struck End Draft Gear Types and Steel Friction Gear on Non-Struck End .....	26
Figure 33. Comparison of Longitudinal Coupler Force and Vertical Coupler Force on Struck End of Car .....	27
Figure 34. Boxplot Comparison of Strain Magnitudes Throughout Test Program .....	28
Figure 35. Boxplot Comparison of Principal Strains Throughout Test Program at Different Locations on Test Car .....	29
Figure 36. Correlation Between Strains and Both Vertical and Longitudinal Coupler Forces ...	30
Figure 37. In-Board Principal Strain versus Coupling Speed for Different Draft Gear Types, Full Tank Car and Three Hopper Cars with Brake on Used as Anvil.....	30
Figure 38. Permanent Shift in Strain Readings During Test Program.....	31
Figure 39. Comparison of Coupling Force During Impact Empty, Half-Full and Full Tank Cars .....	33
Figure 40. Impulse Data Comparison for Various Hammer Configurations and Anvil Configurations with One and Three Hopper Cars with Brakes On .....	34
Figure 41. Impulse Data Comparison for Different Anvil Configurations and Hammer Configurations Using Full and Empty Tank Cars.....	35
Figure 42. Impact Force Data Comparison for Different End-of-Car Units for Given Hammer and Anvil Configurations.....	35

## Tables

---

Table 1. Data Collection System Input Channel List .....	12
Table 3. Test Matrix for Impact Test Program .....	16
Table 4. Various Hammer Configurations, Anvil Configurations and Draft Gear Types Used During the Impact Test Program.....	22
Table 5. $R^2$ for Different Regression Models Based on Different Set of Variables to Predict the Coupling Force.....	25
Table 6. Correlation Coefficient Between Accelerations and Both Vertical and Longitudinal Coupler Forces .....	32
Table 7. Comparison of Impact Force and Impulse (Area Under Force Curve) for Three Impact Tests with Different Weights of Hammer Cars .....	33

## Executive Summary

---

In 2018, the Federal Railroad Administration's (FRA) Office of Research, Development and Technology contracted ENSCO, Inc. to conduct a series of impact tests for different car configurations at various coupling speeds and simulated coupling conditions at Amsted Rail's test facility in Camp Hill, PA. Previous research studies<sup>1</sup> revealed that high magnitude coupling forces that occur in yard operations have the potential to exceed yield limits of mild steel and initiate stub sill damage. The objective of this research study was to characterize the load environment on tank cars during yard operations. The main focus was to identify important factors such as speed and configurations of striking (hammer) and impact absorbing (anvil) cars during impacts to help industry establish yard operation scenarios that cause less damage to tank car stub sills.

A tank car loaned to FRA by Union Tank Car was instrumented with multiple transducers and a data collection system that supported high sampling rates required for conducting impact testing. Impact data for different car configurations, end-of-car units, and coupling speeds were collected. More than 700 impact tests were conducted during which 40 data channels comprised of acceleration, force, speed, and strain data were recorded. This report describes the instrumentation, calibration, testing, and analysis efforts conducted by ENSCO over this testing program period.

After filtering the data to remove invalid data and noise, a statistical analysis was conducted to determine the effect of different parameters on the coupling behavior. Peak longitudinal impact forces measured by the instrumented coupler, impulses at the impact between coupling cars, strains and accelerations were assessed.

The results showed that coupling speed and the type of end-of-car units employed on the cars have the most influence on the peak longitudinal impact force, whereas anvil and hammer configurations have limited effect on the peak impact force. The results also showed that the end-of-car unit type has a limited effect on the transferred energy between impacting cars, whereas hammer and anvil configurations have a considerable effect on the transferred energy. Results also showed that different end-of-car units yielded different in impact forces for different speed ranges. Hydraulic cushioning units yielded lower impact forces than both steel friction and elastomer draft gears did for all speed ranges. Elastomer draft gears yielded lower impact forces than steel friction draft gears for lower coupling speed ranges.

The load characterization results from this research will be combined with fatigue characteristics of stub sill material to design yard operation scenarios that are intended to result in lower stresses in stub sills. The limits on mass and speed combinations should be designed based on the expected life of tank cars. This study documented in this report should serve as the basis for such analysis by documenting impact loading and energy transferred between cars during yard operations, as well as the effect of different factors on impact behavior.

---

<sup>1</sup> Sundaram, N., Martin, T., Selby, B., and González, F. (May 2010). [\*Over-the-Road Testing of the Instrumented Tank Car—A Load Environment Study\*](#). Technical Report, Report No. DOT/FRA/ORD-10/04. Federal Railroad Administration. Washington, DC: U.S. Department of Transportation.

# 1. Introduction

---

This report describes a cooperative test program sponsored by the Federal Railroad Administration (FRA) that was performed by ENSCO, Inc. at Amsted Rail’s test facility in Camp Hill, PA. During these tests impact data was gathered on a test track simulating hump yard operation for train make-up, and the test data was analyzed to improve the understanding of the load environment of tank car stub sills during hump yard operations.

## 1.1 Background

Fractures have been observed on stub sill tank cars for many years. When undetected, these fractures can create a variety of tank car failures. While tank car ruptures are relatively rare, the potential for a catastrophic release of hazardous materials (HAZMAT) has made this a critical issue within the industry. Because of this concern, special requirements for the construction, inspection, and repair of tank cars have been implemented.

Research into the cause of stub sill tank car cracking and propagation continues. It is believed that the fractures are initiated by discrete events resulting in high stresses. Previous research studies conducted by FRA revealed that high magnitude coupling forces that occur in yard operations have the potential to exceed yield limits of mild steel (Sundaram, 2014). The reasons for stub sill failures were primarily attributed to high forces generated in yards initiating damage followed by crack propagation resulting from high vertical coupler force events occurring in mainline operations. High-force events in yards could be mitigated if there was a better understanding of the contributing factors to these high impact loadings during yard operations.

Examples of stub sill fractures observed by CSX Transportation are shown in [Figure 1](#) and [Figure 2](#). As can be seen, these fractures are catastrophic in nature. The tank car industry has design controls in place as specified by the Association of American Railroads’ Manual of Standards and Recommended Practices, Section C Part II–Design, Fabrication and Construction of Freight Cars to ensure that the stub sill to tank reinforcing pad attachment welds fail prior to the reinforcing pad to tank attachment welds.



**Figure 1. Stub Sill Fracture Observed in Callahan, FL, from December 2009 (Sundaram, 2014)**



**Figure 2. Stub Sill Fracture Observed in Charleston, WV, from January 2010 (Sundaram, 2014)**

To better characterize the load environment of the tank car operations in yards, Union Tank Car loaned a tank car to FRA that was instrumented with multiple transducers and a data collection system that supported high sampling rates required for conducting impact testing. Impact data for different car configurations, end-of-car units, and coupling speeds were collected. The tank car used for this effort, provided by Union Tank Car, is shown in [Figure 3](#). A detailed view of the end of the tank car with the stub sill attachment is shown in [Figure 4](#).



**Figure 3. Instrumented Tank Car**



**Figure 4. Detail View of the Stub Sill and Head Brace Attached to the Tank of the Instrumented Tank Car**

This report documents the results and findings, as well as describes the instrumentation, calibration, and testing efforts conducted by ENSCO.

## **1.2 Objectives**

The objective of this research study was to characterize the load environment on tank cars during yard operations. The focus of the study was to identify important factors such as speed and configurations of striking (hammer) and impact absorbing (anvil) cars during impacts to help the industry establish yard operation scenarios that cause less damage to tank car stub sills.

The test used background information and placement of sensors based on results from previous research efforts as well as technical guidance from subject matter experts in the industry (Sundaram, 2014). It is anticipated that the results of this test effort will be used by FRA to establish guidelines for the handling of tank cars during train makeup to minimize damage to the cars prior to revenue service operations. The testing will also make robust, real-world impact load environment data available for further research.

## **1.3 Overall Approach**

To achieve these objectives, a tank car loaned to FRA by Union Tank Car was instrumented with multiple transducers and a data collection system that supported high sampling rates required for conducting impact testing. Impact data for different car configurations, end-of-car units, and coupling speeds were collected during 702 impact tests. The following were recorded during each impact test: 40 data channels comprised of acceleration, force, speed, and strain data. A comprehensive statistical data analysis was conducted on the collected impact data to study the effect of different parameters on the coupling behavior. There were also contributing factors that were identified and assessed to the high impact loadings during yard operations.

## **1.4 Scope**

The scope of this study was limited to conducting a series of impact tests with a tank car for different coupling conditions during yard operation and analysis of the collected data. This report serves as an aid for designing safe yard operation scenarios by providing information on the extent of impact loading and energy transferred during yard operations as well as the effect of different factors on impact behavior.

## **1.5 Organization of the Report**

[Section 2](#) discusses the test methodology, which includes a review of the instrumented tank car, different sensors used during the test program, and the test track that was used for conducting the impact tests. [Section 2](#) also details the impact test matrix and different test scenarios considered for the testing program. [Section 3](#) presents the results of the test data analysis and includes observations for the respective analysis sections, and [Section 4](#) provides a summary on the work performed and the results.

## 2. Test Methodology

---

This section describes the instrumented tank car, the different sensors used during the test program, and the test track that was used for conducting the impact tests. This section also details the impact test matrix and different test scenarios considered during the testing program.

### 2.1 Instrumented Tank Car

A tank car loaned to FRA by Union Tank Car was instrumented with multiple transducers and a data collection system that supported high sampling rates required for conducting impact testing. The instrumented tank car was equipped with instrumented couplers on both ends of the car, a vertical coupler force measurement system, multiple accelerometers, and multiple rosette strain gages at different locations around stub sills that were identified as the high stress locations for the test program. [Figure 5](#) shows a schematic of the test tank car's instrumentation.

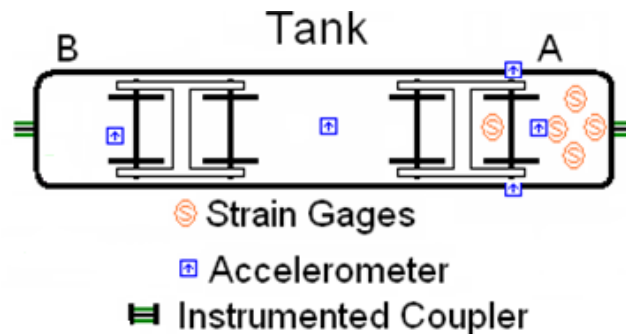


Figure 5. Schematic Diagram of Tank Car's Instrumentation

#### 2.1.1 Coupler Forces

Longitudinal coupler forces were measured on both the A-end and B-end of the tank car. Two instrumented couplers outfitted with strain gauge bridges were used to measure the longitudinal forces. [Figure 6](#) shows an image of instrumented coupler installed on the A-end of the car.



Figure 6. Instrumented Coupler for Measuring Longitudinal Coupler Forces

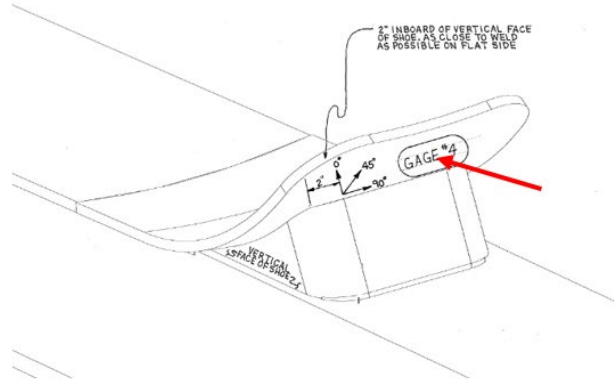
To measure vertical forces, a pair of shear strain gauges were mounted on each side of the stub sill, as shown in [Figure 7](#). The shear strain gauges were wired using a completion card to form a full bridge. The mounting process included grinding and polishing the coupler surface to provide a smooth area to which the strain gauges were welded. Room temperature vulcanized (RTV) silicone rubber coatings were used as protective and waterproofing coatings. These shear strain gauges were applied only on the A-end of the instrumented tank car. The black gauges on the left were used during this testing. The gauges on the right installed during previous phases of testing were not used for this impact testing.



**Figure 7. Shear Strain Gages Installed on the Stub Sill for Measuring Vertical Coupler Force**

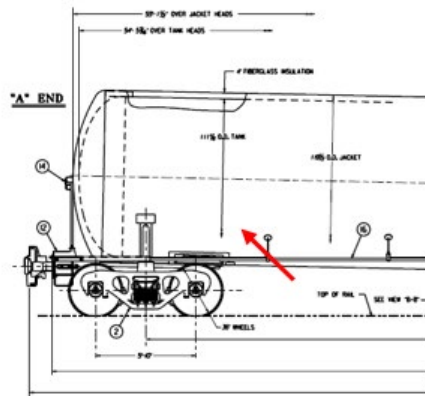
### **2.1.2 Strain Gages**

Five sets of rosette strain gages were installed on various locations around the stub sill on the A-end (striking end) of the car. These locations were identified as the high stress areas during a consultation with FRA and Union Tank Car's subject matter experts. To determine the principal stresses, three individual strain gauges were installed 45 degrees apart to form a rosette. [Figure 8](#) shows the rosette strain gage installed on the shoulder pad centered above the head shoe. The bottom three gauges were used during this testing. The top three gauges were installed during previous testing and were not used for this investigation.



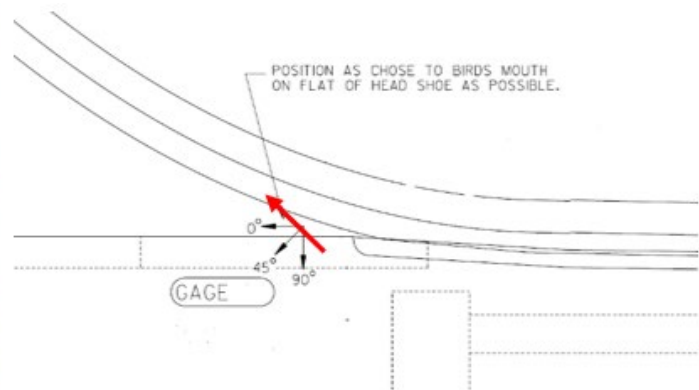
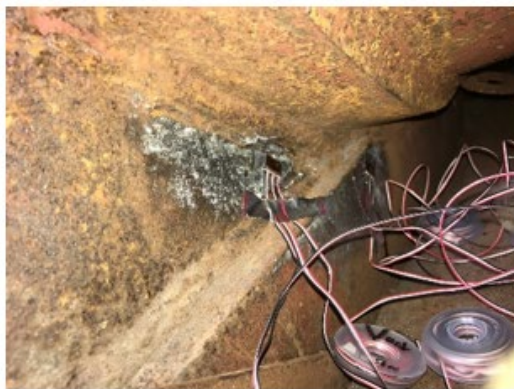
**Figure 8. Shoulder Pad Strain Gage Installed Above the Head Shoe at the A-End of the Instrumented Tank Car**

Figure 9 shows the rosette strain gage installed under the car at the end of the stub sill. This gage is referred to as the in-board strain gage.



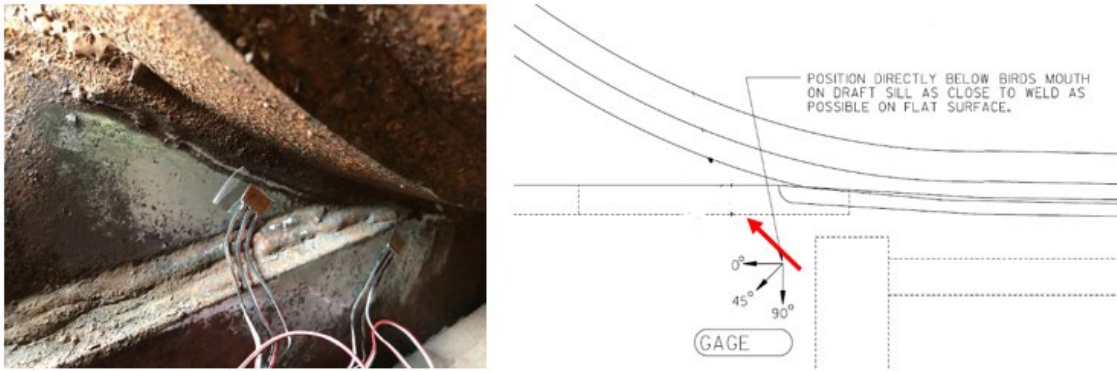
**Figure 9. In-Board Strain Gage Installed Under the Car at the End of the Stub Sill Beam**

Figure 10 shows the rosette strain gage installed on the head shoe close to a corner weld. This gage is referred to as the head shoe strain gage.



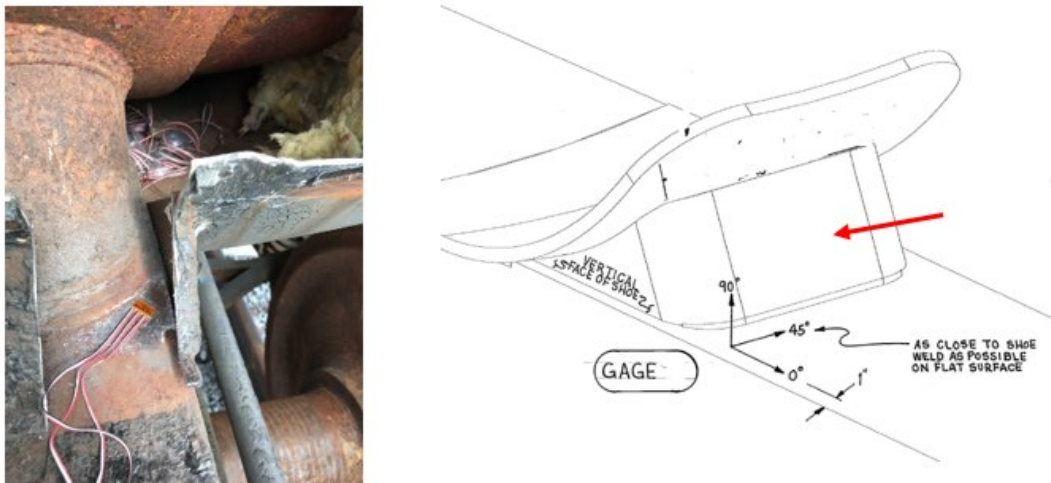
**Figure 10. Strain Gage Installed on the Head Shoe Close to the Corner**

Figure 11 shows the rosette strain gage installed on the stub sill below the head shoe strain gage close to draft gear's rear stop. This gage is referred to as the stub sill stop strain gage.



**Figure 11. Strain Gage Installed on the Stub Sill Close to the Rear Stop**

Figure 12 shows the rosette strain gage installed on top of the stub sill close to the head shoe. This gage is referred to as the head brace strain gage.



**Figure 12. Strain Gage Installed on Top of the Stub Sill Close to the Head Shoe**

### 2.1.3 Accelerometers

Accelerometers were installed at several locations on the tank car. A tri-axial accelerometer mounted on top of the carbody (Figure 13) measured accelerations in longitudinal, lateral and vertical directions. Two dual axis accelerometers, mounted on the stub sill at each end of the car (Figure 14), measured accelerations in the longitudinal and vertical directions. In addition to ENSCO's accelerometers, Amsted Rail installed three triaxial accelerometers at the top of the carbody and on the stub sill at each end of the car.

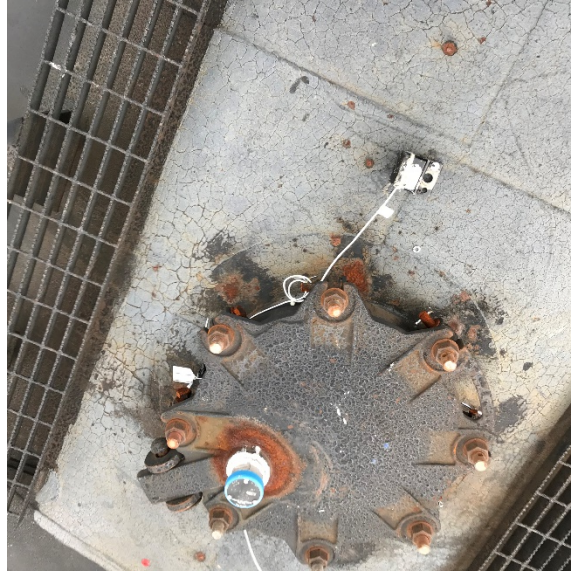


**Figure 13. Tri-Axial Accelerometer Mounted on Top of the Carbody**



**Figure 14. Dual-Axis Accelerometer Mounted on the Stub Sill on Each End of the Car**

#### **2.1.4 Other Transducers**

In addition, other transducers such as laser speedometer for measuring the coupling speed, temperature sensor, and humidity sensors were used to collect data. The coupling force was recorded on an instrumented coupler installed on Amsted's rail car. The acceleration of the carbody and stub sill on each end was also recorded by tri-axial accelerometers installed on the tank car by Amsted Rail.

### 2.1.5 Data Acquisition and Hardware Settings

Data was collected using National Instrument's PCIe6353 Data Acquisition Card. The card supported 32 input analog channels with 16-bit resolution. The collection system recorded 27 channels of data at a rate of 10 kHz. A low-pass anti-aliasing, fourth order Butterworth filter was implemented with a Sallen-Key Topology filter board to filter the input data with a cut-off frequency of 1,000 Hz. A Nuvo-5095GC ruggedized computer collected and stored data through LabView software. The system was equipped with +/- 5 V and +/- 12 V power supply for providing clean power to transducers. Figure 15 shows the junction box that was installed to the side of the tank car. The box contained the computer, acquisition hardware, power supply, analog filter board, and terminal blocks for signal routing and distribution.

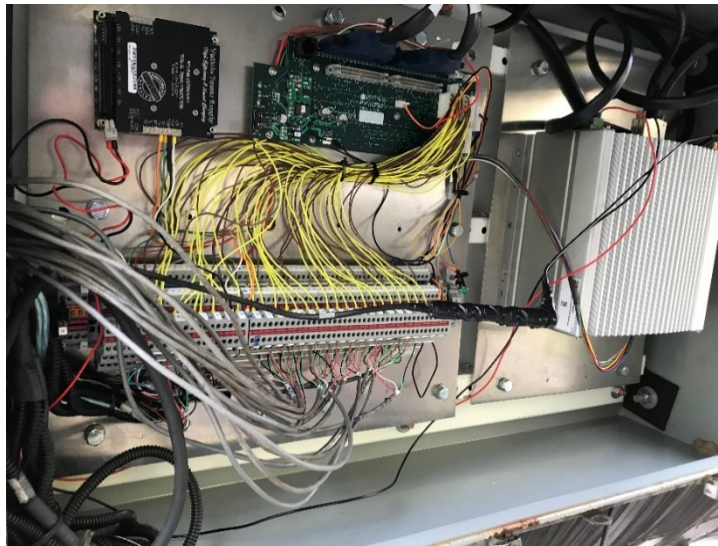


**Figure 15. Junction Box with Data Collection System Hardware**

Four 115 W, 12 V solar modules solar panels and a set of 110 Ah, 12 V AGM batteries were used to power the system. Figure 16 shows the solar panels and the battery box. The battery box also contained the electronics that controlled battery charging.



**Figure 16. Solar Panel and Battery Box on Top of the Instrumented Tank Car**

### 2.1.6 Channel Assignments

Assignments and descriptions of each channel are shown in Table 1. In addition to channels listed in Table 1, Amsted’s data acquisition system recorded coupling speed, environment temperature, humidity, instrumented coupler output, and nine acceleration channels.

**Table 1. Data Collection System Input Channel List**

Channel Number	Description	Units
1	Carbody Longitudinal Accelerations	[g]
2	Carbody Vertical Accelerations	[g]
3	Carbody Lateral Accelerations	[g]
4	Stub Sill Vertical Accelerations on B End	[g]
5	Stub Sill Longitudinal Accelerations B-End	[g]
6	Stub Sill Vertical Accelerations on A-End	[g]
7	Stub Sill Lateral Accelerations A-End	[g]
8	Axle Vertical Accelerations on right Side A-End	[g]
9	Stub Sill Longitudinal Accelerations A-End	[g]
10	Longitudinal Coupler Force A-End	[ $\mu\epsilon$ ]
11	Longitudinal Coupler Force B-End	[ $\mu\epsilon$ ]
12–14	Rosette Strain Gage at Shoulder Pad Location— 45/Vertical/+45	[ $\mu\epsilon$ ]
15	Vertical Coupler Force A-End	[ $\mu\epsilon$ ]
16–18	Rosette Strain Gage at Stub Sill Stop Location— Horizontal/45/Vertical	[ $\mu\epsilon$ ]
19–21	Rosette Strain Gage at Head Shoe Location— Horizontal/45/Vertical	[ $\mu\epsilon$ ]
22–24	Rosette Strain Gage at Head Brace Location— Longitudinal/45/Lateral	[ $\mu\epsilon$ ]
25–27	Rosette Strain Gage at In-Board Location— Longitudinal/45/Lateral	[ $\mu\epsilon$ ]
28–29	Spare Channel	N/A
30	Battery Voltage Monitor	V
31–32	+/- 5 Volt Power Monitor	V

### 2.1.7 Sensor Calibration

All instrumentation was calibrated prior to testing. Portable sensors, including accelerometers and longitudinal force bridges on the instrumented couplers, were calibrated in a laboratory prior

to installation on the vehicle. The vertical force bridges on the coupler that converted strains to forces required field calibration.

The vertical coupler force was calibrated in the field using a custom load fixture consisting of a metal frame, a calibrated load cell and a hydraulic ram to apply vertical loads. Figure 17 shows the calibration fixture when downward (left) and upward (right) vertical forces were applied.



Figure 17. Vertical Coupler Force Calibration Setup

The applied force and the strain gauges' full bridge were measured at several points for both upward and downward loadings. The procedure was conducted three times. Figure 18 shows a graph of the calibration results for the vertical coupler force.

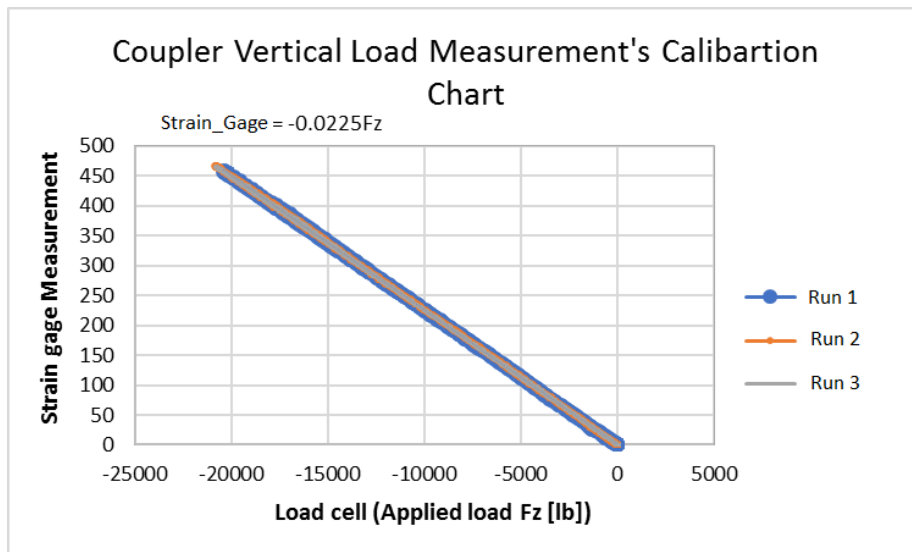


Figure 18. Vertical Coupler Force Calibration Results

### 2.1.8 Tank Car Weights

To collect information at various tank car weights, the tank car was filled with water throughout the program. The weight of the car with an empty tank was 78.1 kips. The tank car was empty for the initial series of tests. On January 25, 2018, the tank car was partially filled with 101 kips of water, resulting in a 179.4-kip tank car. On February 1, 2018, the tank car was loaded with an additional 84 kips of water resulting in a fully loaded tank carload of 263.2 kips. Towards the end of the test program, on May 25, 2018, the water in the tank car was released to finish the remaining tests with an empty tank car. [Table 2](#) shows the schedule for the weight of the tank car during the test program.

**Table 2. Tank Car Weights Throughout Test Program**

Dates		Water Weight	Total Tank Car Weight
From	To	[kips]	[kips]
1/9/2018	1/25/2018	0	78.1
1/26/2018	2/1/2018	101.3	179.4
2/2/2018	5/25/2018	185.1	263.2
5/25/2018	6/7/2018	0	78.1

### 2.2 Impact Test Program

The impact test program was conducted on Amsted Rail’s test track between January 2018 and June 2018. The test program included a series of impact tests for different car configurations, end-of-car units, and coupling speeds that are detailed in [Section 2.3](#). [Figure 19](#) shows the instrumented tank car at Amsted’s test track.

To initiate the impact, the blue bogie coupled to the tank car was attached to a winch that was used to pull the vehicle up a hill. When the car reached the proper position for the intended impact speed, it was released sending the car into the rest of the test vehicles. This simulated the real-world hump yard operation used for making up trains. In impact testing of this nature, the striking car that is in motion is referred to as the hammer and the stationary cars that are parked down the hill are referred to as the anvil.



**Figure 19. Instrumented Tank Car at the Amsted Test Track**

### **2.3 Test Matrix and Data Collected**

A comprehensive test matrix was established to test various coupling conditions and car configurations during yard operations. The test matrix included:

- Different tank car weights—empty, partially loaded, and fully loaded with water
- Different end-of-car units—steel friction draft gear, elastomer draft gear, and hydraulic cushioning units
- Different anvil configurations—one car with brakes on, one car with brakes off, and 4 cars with brakes on
- Multiple coupling speeds—target speeds of 4, 6, 7, 7.5, 8, 9 and 10 mph

[Table 3](#) shows the detailed test matrix that was used for the impact test program.

**Table 2. Test Matrix for Impact Test Program**

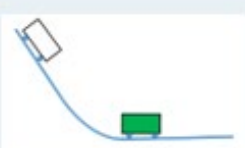
A	Layout (Green car is the instrumented car)	Loaded/Empty	Axle	Anvil Car's Hand Brake	Speed					Draft Gear			
					4	6	7.5	8	10	90:1	90:3	92:18/D	
1		Empty	Full	No	Red						Red		
2		Empty	Full	No	Red						Red		
3		Empty	Full	Yes	Red						Red		
4		Empty	Full	Yes	Red	Red					Red		
5		Empty	Full	Yes	Red		Red				Red		
6		Empty	Full	Yes	Red			Red			Red		
7		Empty	Full	Yes	Red				Red		Red		
8		Empty	Full	Yes	Red					Red	Red		
9		Partially Full	Full	No	Red						Red		
10		Partially Full	Full	No	Red						Red		
11		Partially Full	Full	Yes	Red						Red		
12		Partially Full	Full	Yes	Red	Red					Red		
13		Partially Full	Full	Yes	Red		Red				Red		
14		Partially Full	Full	Yes	Red			Red			Red		
15		Partially Full	Full	Yes	Red				Red		Red		
16		Partially Full	Full	Yes	Red					Red	Red		
17		Full	Full	No	Red						Red		
18		Full	Full	No	Red						Red		
19		Full	Full	Yes	Red						Red		
20		Full	Full	Yes	Red	Red					Red		
21		Full	Full	Yes	Red		Red				Red		
22		Full	Full	Yes	Red			Red			Red		
23		Full	Full	Yes	Red				Red		Red		
24		Full	Full	Yes	Red					Red	Red		
25		Empty	Full	Yes	Red					Red			
26		Empty	Full	Yes	Red						Red		
27		Empty	Full	Yes	Red	Red					Red		
28		Empty	Full	Yes	Red		Red				Red		
29		Empty	Full	Yes	Red			Red			Red		
30		Empty	Full	Yes	Red				Red		Red		
31		Partially Full	Full	Yes	Red					Red	Red		
32		Partially Full	Full	Yes	Red	Red					Red		
33		Partially Full	Full	Yes	Red		Red				Red		
34		Partially Full	Full	Yes	Red			Red			Red		
35		Partially Full	Full	Yes	Red				Red		Red		
36		Partially Full	Full	Yes	Red					Red	Red		
37		Full	Full	Yes	Red						Red		
38		Full	Full	Yes	Red	Red					Red		
39		Full	Full	Yes	Red		Red				Red		
40		Full	Full	Yes	Red			Red			Red		
41		Full	Full	Yes	Red				Red		Red		
42		Full	Full	Yes	Red					Red	Red		
43		Full	Full	Yes	Red	Red					Red		
44		Full	Full	Yes	Red		Red				Red		
45		Full	Full	Yes	Red			Red			Red		
46		Full	Full	Yes	Red				Red		Red		
47		Full	Full	Yes	Red					Red	Red		
48		Full	Full	Yes	Red						Red		
49	Full	Full	Yes	Red	Red					Red			
50	Full	Full	Yes	Red		Red				Red			
51	Full	Full	Yes	Red			Red			Red			
52	Full	Full	Yes	Red				Red		Red			
53	Full	Full	Yes	Red					Red	Red			
54	Full	Full	Yes	Red						Red			
55		The instrumented tank car will be turned (orientation changed)				Red					Red		
56		Full	Full	Yes	Red	Red					Red		
57		Full	Full	Yes	Red		Red				Red		
58		Full	Full	Yes	Red			Red			Red		
59		Full	Full	Yes	Red				Red		Red		
60		Full	Full	Yes	Red					Red	Red		
61		Full	Full	Yes	Red	Red					Red		
62		Full	Full	Yes	Red		Red				Red		
63		Full	Full	Yes	Red			Red			Red		
64		Full	Full	Yes	Red				Red		Red		
65		Full	Full	Yes	Red					Red	Red		
66		Full	Full	Yes	Red						Red		
67		Full	Full	Yes	Red	Red					Red		
68		Full	Full	Yes	Red		Red				Red		
69	Full	Full	Yes	Red			Red			Red			
70	Full	Full	Yes	Red				Red		Red			
71	Full	Full	Yes	Red					Red	Red			
72	Full	Full	Yes	Red						Red			
73		Full	Full	Yes	Red					Red			
74		Full	Full	Yes	Red	Red					Red		
75		Full	Full	Yes	Red		Red				Red		
76		Full	Full	Yes	Red			Red			Red		
77		Full	Full	Yes	Red				Red		Red		
78		Full	Full	Yes	Red					Red	Red		
79		Full	Full	Yes	Red						Red		
80		Full	Full	Yes	Red	Red					Red		
81		Full	Full	Yes	Red		Red				Red		
82		Full	Full	Yes	Red			Red			Red		
83		Full	Full	Yes	Red				Red		Red		
84		Full	Full	Yes	Red					Red	Red		
85		Full	Full	Yes	Red						Red		
86		Full	Full	Yes	Red	Red					Red		
87	Full	Full	Yes	Red		Red				Red			
88	Full	Full	Yes	Red			Red			Red			
89	Full	Full	Yes	Red				Red		Red			
90	Full	Full	Yes	Red					Red	Red			
91	Full	Empty	Yes	Red						Red			
92	Full	Empty	Yes	Red	Red					Red			
93	Full	Empty	Yes	Red		Red				Red			
94	Full	Empty	Yes	Red			Red			Red			
95	Full	Empty	Yes	Red				Red		Red			
96	Full	Empty	Yes	Red					Red	Red			

Table 3 shows the schematic diagrams for different layouts used in the test program. During the impact test program, more than 700 impact tests were conducted. For each impact test, approximately 40 data channels comprised of acceleration, force, speed, and strain data were recorded. The green car shown in the schematics within Table 3 indicates the instrumented tank car. The Amsted test track was not capable of conducting impact tests with more than one hammer car.

During the test program, different end-of-car units were tested. These are shock-absorbing devices, also referred to as draft gear, that while under stress increase the free movement of adjoining coupler cars as the train is started or stopped. Draft gears cushion the impact of coupling cars during hump yard operations during the make-up of trains, as well as absorb energy associated with in-train forces due to slack motion during train movements. Draft gears absorb energy in both pulling and pushing directions.

Figure 20 illustrates the three types of draft gears used during the test program. 901E steel friction draft gear (left) contains steel wedges that are geometrically arranged to absorb the coupler force using the stick-slip phenomena. The steel friction gear provides a maximum travel of 3 inches. 901G elastomer friction gear (middle) consists of elastomer pads that absorb energy via hysteresis. The elastomer friction gears also provide a maximum travel of 3 inches. Hydraulic cushioning units (right) absorb energy by pushing hydraulic fluid through specially designed valves based on viscous friction. The hydraulic units provide travel of more than 10 inches.



Figure 20. Draft Gears Used During Impact Test Program

## 2.4 Issues Encountered During Testing

Several issues occurred during the testing:

- Some of the accelerometers failed during the testing. They were replaced with calibrated and functioning sensors.
- The battery box fixture, due to the extent of the testing and large impacts, got weakened throughout the testing. This caused multiple failure of the battery box to provide power to the system. The problems were fixed during the testing.
- One of the channels of the head shoe gage set failed toward the end of the testing program, which was not fixed.

These were all minor issues and did not affect the overall test results.

### 3. Impact Test Data Analysis and Results

---

The purpose of this chapter is to provide an overview of the results determined from analysis of the data collected during the test program. After filtering the data to remove invalid data and noise, a statistical analysis conducted to study the effect of different parameters on the coupling behavior. The peak longitudinal impact force measured by the instrumented coupler was assessed. In addition to coupling force, the impulse at the impact between coupling cars was studied. These are discussed in detail in the following sections.

#### 3.1 Filtering Data

After collecting data, the data was processed to filter out invalid data and noise. In total, there were approximately 28,000 data signals (702 tests at 40 channels each). First, all the recorded data were manually and visually checked to remove any invalid data associated with failures of the power system, data collection system or individual sensors.

After manual review of the data, the data was filtered to remove noise. The data collection sampling rate during testing was 10 kHz and it was equipped with an analog anti-aliasing, fourth order Butterworth, low pass filter with a cut-off frequency of 1 kHz. The recorded data was further filtered with a digital low pass filter. Different cut-off frequencies for the digital low pass filter were investigated. [Figure 21](#) shows a sample of longitudinal coupler force data resulting from use of different low pass filters.  $F_c$  represents the cut-off frequency in Hz for different low pass filters and  $max$  represents the maximum coupler force in kips calculated after filtering the data. As shown in [Figure 21](#), low pass filters with cut-off frequency of 60 Hz or higher do not significantly affect the maximum force reading. In addition to maximum coupler force, the frequency content of the signal and noise were considered for selecting the digital low pass filter cut-off frequency. To this end, the time domain signal is divided into impact signal and noise floor signal as shown in [Figure 21](#). Then, the frequency content of the noise and impact signals were obtained. [Figure 22](#) shows the frequency content of the impact signal and noise floor signal, respectively. A clear peak at 100 Hz in the noise floor signal was dominant. The source of this noise was attributed to the data collection system or leakage through the shielding of the cables. A cut-off frequency of 60 Hz was chosen for the digital low pass filter to increase the signal-to-noise ratio. This cut-off frequency reduced the peak in the noise floor frequency content but did not significantly affect the maximum force reading.

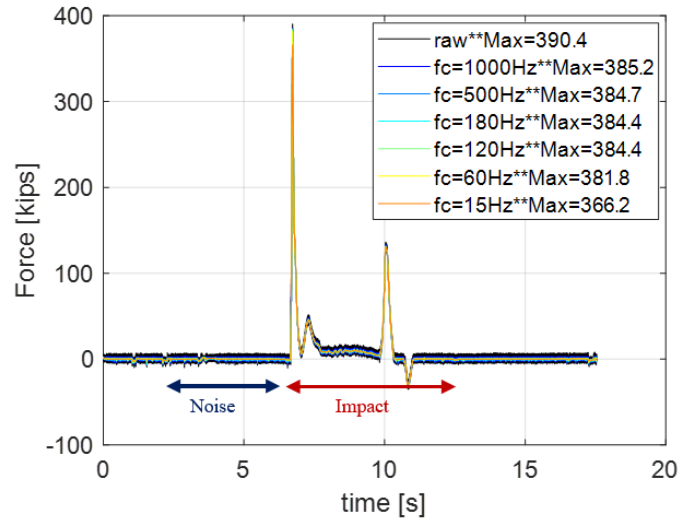


**Figure 21. Sample Longitudinal Coupler Force with Different Low Pass Filters in Time Domain**

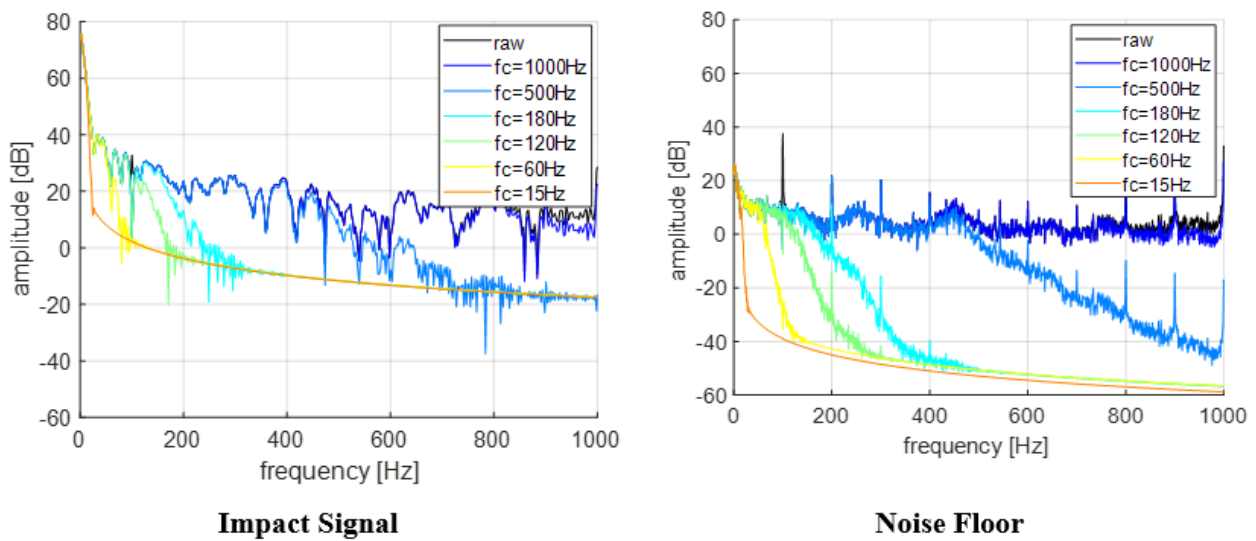


**Figure 22. Impact Signal and Noise Floor Frequency Contents with Different Low Pass Filters**

As shown in [Figure 23](#), invalid spikes were frequently observed in the speed signal. In addition to low pass filter for the force, as well as acceleration and strain gage signals, a median filter was used to remove spikes in the speed signal as shown in [Figure 23](#).

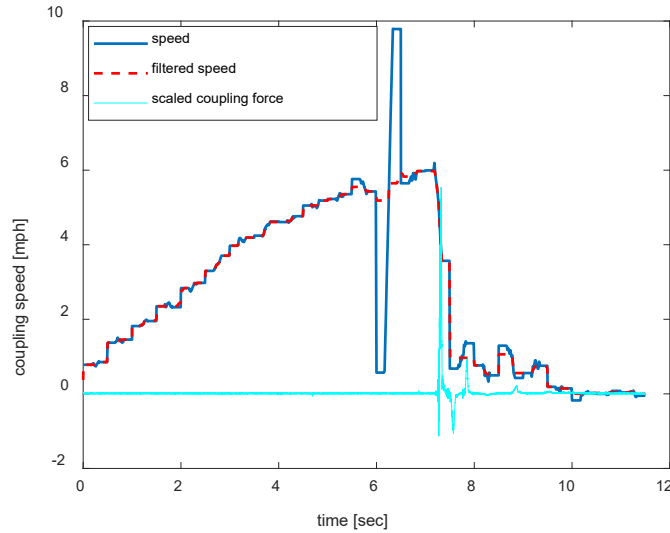


**Figure 23. Median Filtering Used for Removing Invalid Spikes in the Speed Signal**

### 3.2 Secondary Impact

Amsted’s test track did not allow for impact tests with more than one car as the hammer. So, the test matrix (Table 3) did not include any test layout with a two-car hammer. However, the collected impact test data were used to obtain impact force-speed data for configurations with two-car hammers as shown in Figure 24. In these scenarios, a back-up string of cars was parked 10 feet behind the anvil car. The hammer car would travel down the hill, couple into the anvil car and then the resulting two-car consist would strike the string of parked cars. This would result in two impacts on the original anvil car where the secondary impact was caused by the two cars striking the parked cars.

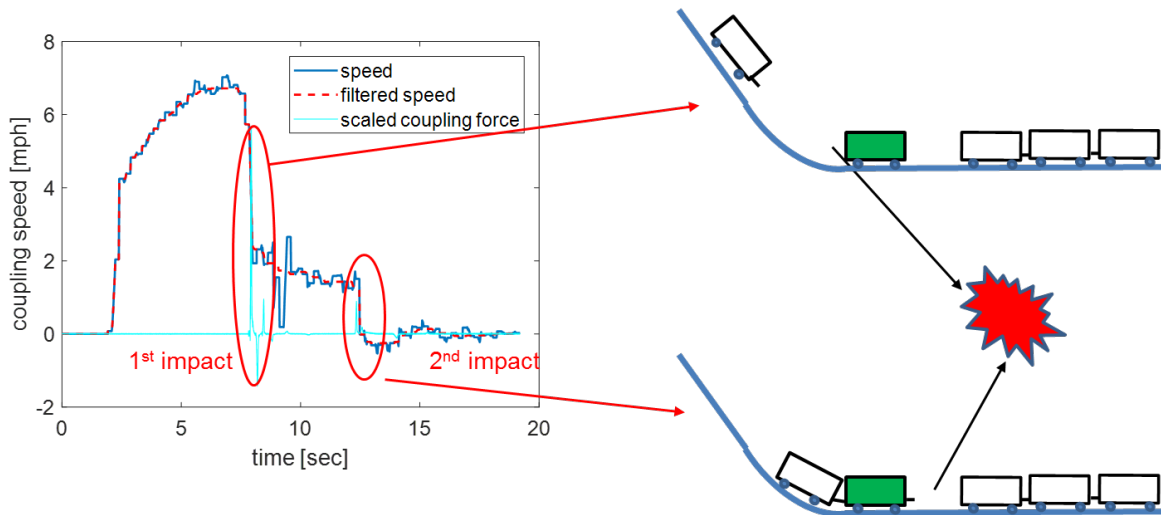


**Figure 24. Arrangement of Test Cars Resulting in Secondary Impacts with Multiple Hammer Cars**

There were 103 tests with recorded secondary impacts. [Figure 25](#) shows coupler force versus coupling speed for different hammer configurations for these secondary impacts. The coupling speed for the secondary impact data is always relatively low due to the test procedure.

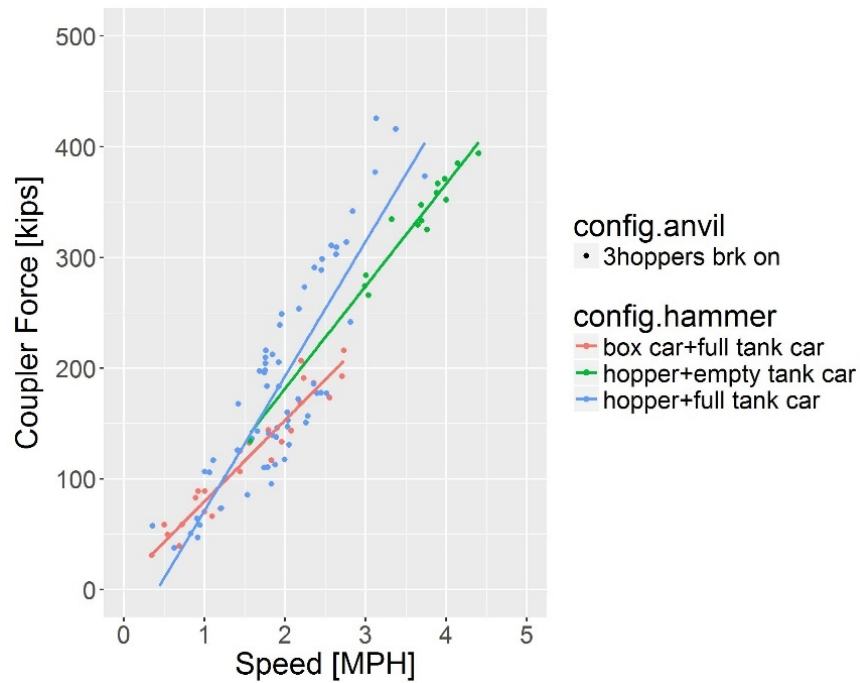


**Figure 25. Coupling Force versus Coupling Speed for Secondary Impacts**

### 3.3 Force Data Analysis

After filtering the data to remove invalid measurements and noise, a statistical analysis conducted to study the effect of different parameters on the coupling behavior. An assessment took place of peak longitudinal impact force measured by the instrumented couplers.

[Figure 26](#) shows longitudinal coupler force during impact versus coupling speed with various anvil and hammer configurations as well as draft gear types. The y-axis of each subplot represents the struck end coupler force with a maximum value of 1,500 kips. The x-axis of each subplot is the coupling speed up to about 10 mph. Columns of subplots represent different hammer configurations and individual rows reflect different anvil configurations. Results collected for different draft gear types are represented by different colors.

[Table 4](#) shows the list of hammer configurations, anvil configurations and draft gear types employed in the program. [Figure 26](#) indicates that there are some patterns in the results representing the effect of draft gear type, anvil configuration, and hammer configuration on the coupler force. These effects are addressed individually in the remainder of this section.

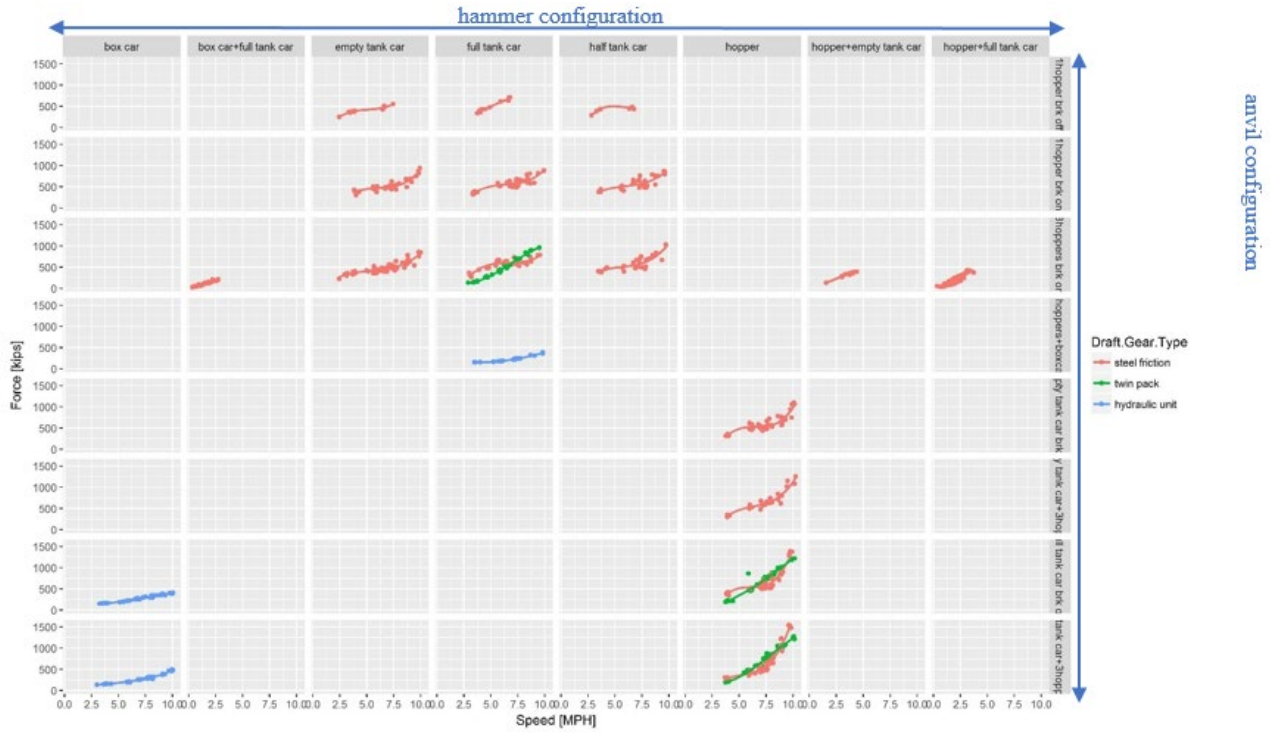
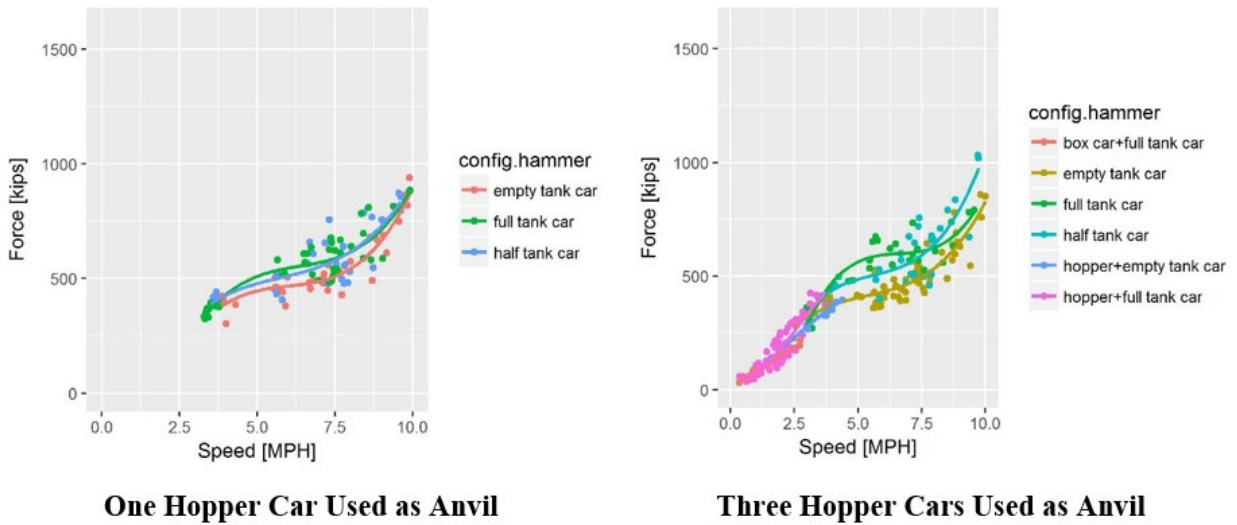


**Figure 26. Coupling Force versus Coupling Speed Plots for Different Coupling Conditions During the Impact Test Program**

**Table 3. Various Hammer Configurations, Anvil Configurations and Draft Gear Types Used During the Impact Test Program**

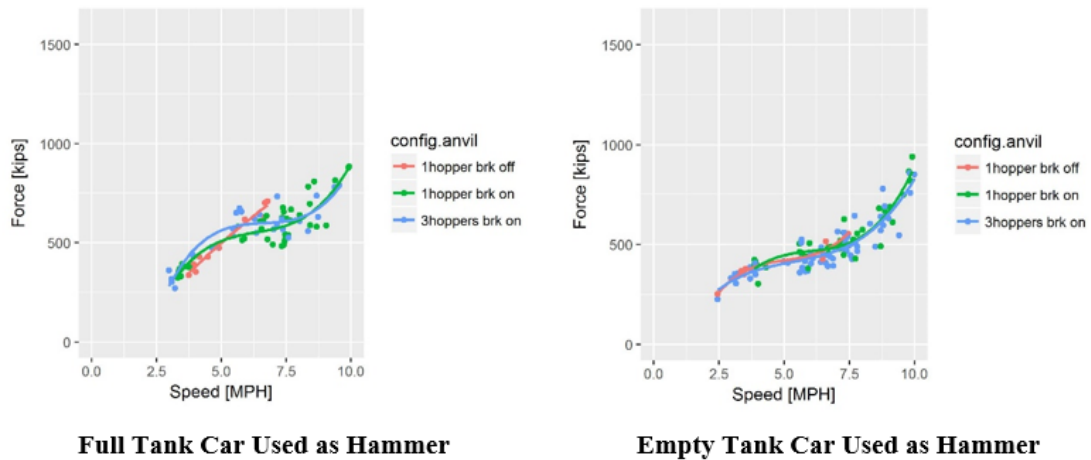
Hammer Configurations	Anvil Configurations	Draft Gear Types
Box Car	1 Hopper Car, Brake Off	Steel Friction
Box Car + Full Tank Car	1 Hopper Car, Brake On	Elastomer
Empty Tank Car	3 Hopper Cars, Brake On	Hydraulic Unit
Full Tank Car	3 Hopper Cars + Box Car	
Half Tank Car (Partially Loaded)	Empty Tank Car, Brake On	
Hopper Car	Empty Tank Car + 3 Hopper Cars	
Hopper Car + Empty Tank Car	Full Tank Car, Brake On	
Hopper Car + Full Tank Car	Full Tank Car + 3 Hopper Cars	

Figure 27 shows impact force data for various hammer configurations and anvil configurations with one hopper car and the brake applied (left), and with three hopper cars and the brakes applied (right). Tank cars of different weights were used to create the different hammer configurations. The results show that the weight of the hammer tank car has a limited effect on the peak impact force.



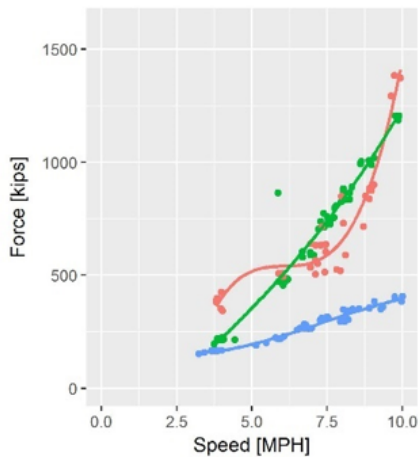
**Figure 27. Impact Force Data Comparison for Different Hammer Configurations and Anvil Configurations with One and Three Hopper Cars**

Figure 28 shows impact force data for various anvil configurations and hammer configurations using a full tank car (left) and an empty tank car (right). Different consists were used to create different anvil configurations. The results indicate that the anvil configurations, similar to hammer configurations, have a limited effect on the peak impact force.

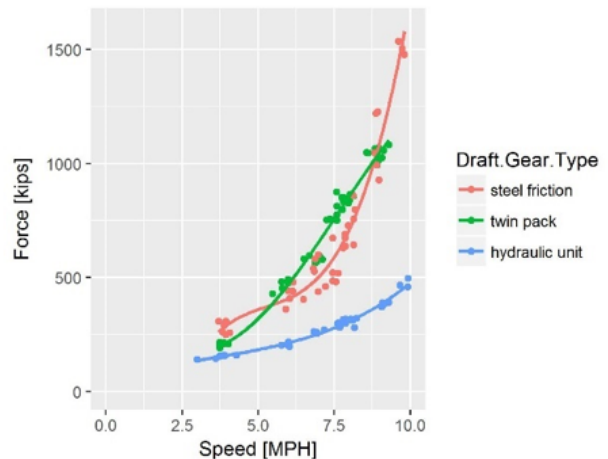


**Figure 28. Impact Force Data Comparison for Different Anvil Configurations Using Full and Empty Tank Cars as Hammer**

Figure 29 shows impact force data for given hammer and anvil configurations using different end-of-car units. The anvil configuration was a full tank car with the brake applied (left) and a full tank car plus three hopper cars (right). The results show that the various end-of-car units perform differently with respect to impact force for different speed ranges. The hydraulic cushioning unit dampened more impact force than both steel friction and elastomer draft gears for all speed ranges. The elastomer draft gear dampened more impact force than the steel friction draft gears performed at low coupling speeds. The peak force started to increase rapidly in steel friction draft gears for coupling speeds of approximately 6.5 mph.



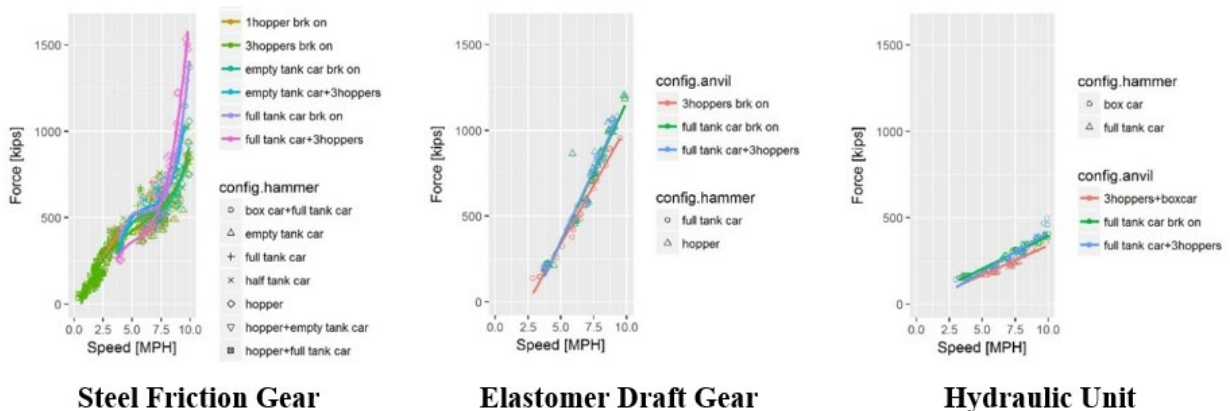
**Full Tank Car with Brake Applied Used as Anvil**



**Full Tank Car and Three Hopper Cars with Brake Applied Used as Anvil**

**Figure 29. Impact Force Data Comparison for Different End-of-Car Units for a Given Hammer and Anvil Configurations Using Full Tank Car and Full Tank Car Plus Three Hopper Cars**

Figure 30 compares all the impact force data for steel friction (left), elastomer draft gear (middle) and hydraulic unit (right). Results for the elastomer draft gear and hydraulic unit were very consistent. However, impact forces when steel friction draft gear was used was more scattered. This is likely due to the highly nonlinear nature of stick-slip behavior within the steel friction gears.



**Steel Friction Gear**

**Elastomer Draft Gear**

**Hydraulic Unit**

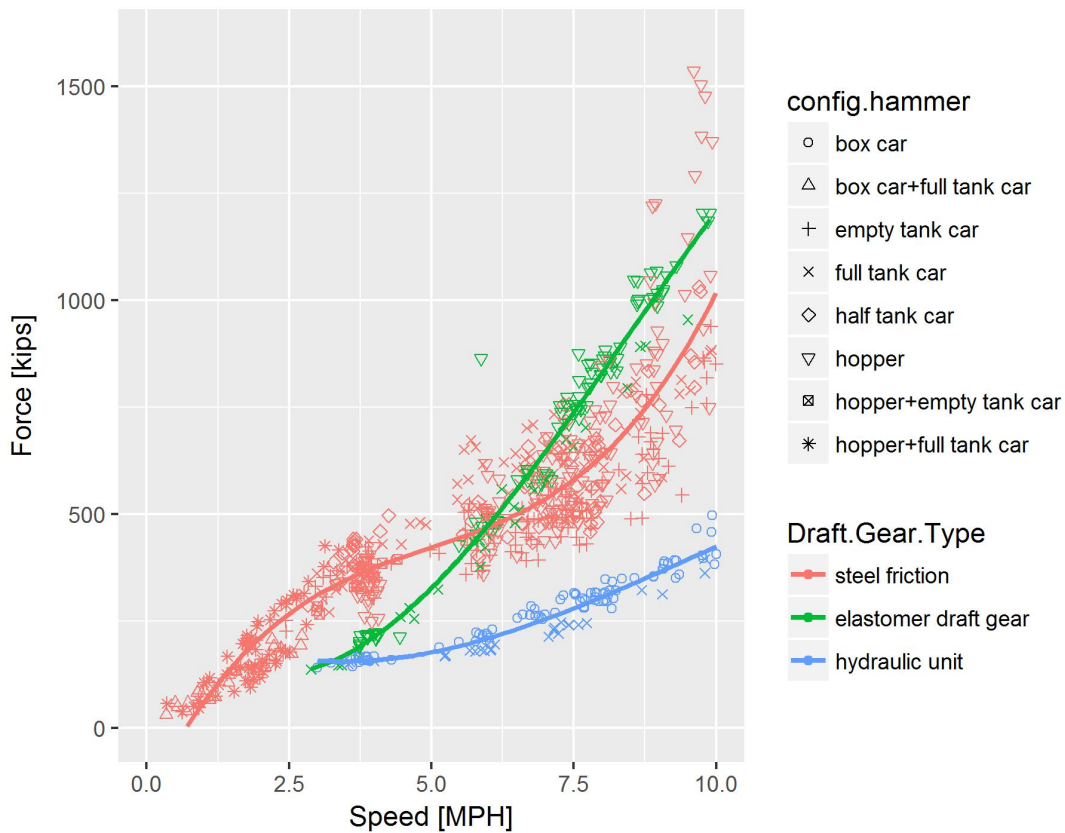
**Figure 30. Impact Force Data Comparisons for Different End-of-Car Units**

The results showed that the maximum longitudinal coupler force during impact is mainly affected by draft gear type and coupling speed. Other coupling conditions such as anvil configuration, hammer configuration or environmental conditions have a limited effect on the coupler force. Various regression models for explaining coupler force using different sets of variables, or predictors, were constructed. The coefficient of determination ( $R^2$ ) was used to compare the regression models, this is a measure of how well observed outcomes are replicated by the model based on the proportion of total variation of outcomes explained by the model. Table 5 shows the  $R^2$  results calculated for different regression models. The results show that

most of the variability in the force data is explained by considering speed, gear type, hammer configuration, anvil configuration, temperature, and humidity.

**Table 4. R<sup>2</sup> for Different Regression Models Based on Different Set of Variables to Predict the Coupling Force**

Variables	R <sup>2</sup>
All	0.81
Speed	0.56
Speed + Gear	0.79
Speed + Hammer	0.75
Speed + Anvil	0.61
Speed + Temperature	0.56
Speed + Humidity	0.57
Speed + Gear + Hammer	0.80
Speed + Gear + Anvil	0.80



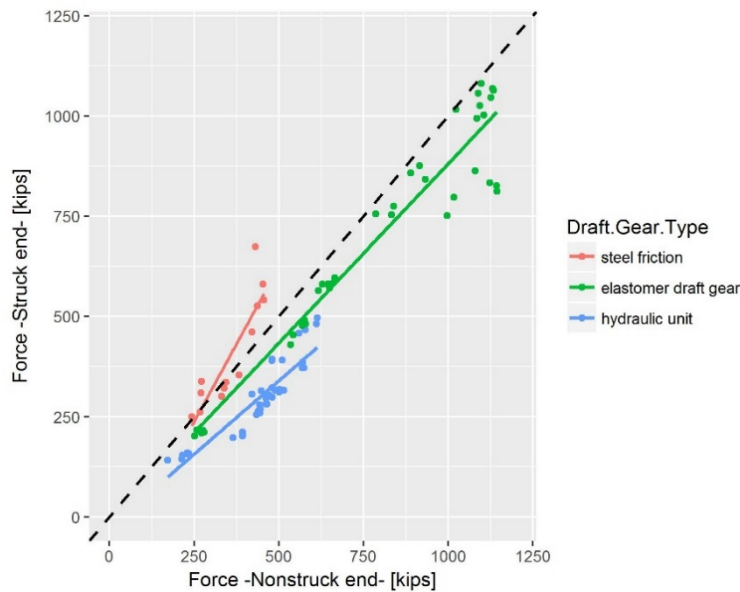
**Figure 31. Coupler Force versus Speed for All Impact Tests**

Figure 31 shows coupler force versus speed variations for all impact tests during the test program. The best regression line for each draft gear type as a function of coupling speed is calculated as:

$$\begin{cases} \text{steel friction} : F = 166 + 267.7 \times V - 45.2 \times V^2 + 3 \times V^3 \\ \text{elstomer draft gear} : F = 459 + 161.9 \times V \\ \text{hydraulic unit} : F = 20 + 41.7 \times V \end{cases}$$

where  $V$  is the coupling speed and  $F$  is the maximum coupler force during impact. Results show that a polynomial of degree 3 best defines the coupling force as a function of coupling speed for steel friction draft gears. For elastomer draft gear and hydraulic unit, a linear regression line best defines the relationship.

In addition to the instrumented coupler on the striking end of the tank car (A-end), the tank car was equipped with another instrumented coupler on the B-end of the car. Measurements from the instrumented couplers on both the striking end of the tank car (A-end) and the B-end of the tank car were studied. Figure 32 compares longitudinal impact force between “struck” and “non-struck” ends of the car. The results show that the non-struck end forces are comparable to struck end forces, indicating that the impact force passes through the anvil consist. Thus, all the cars in the anvil consist experience the impact force.



**Figure 32. Comparison of Struck and Non-Struck End Impact Force for Different Struck End Draft Gear Types and Steel Friction Gear on Non-Struck End**

The results shown in Figure 32 indicates that if there is elastomer draft gear or hydraulic units in the struck end and steel friction draft gear in the non-struck end, the non-struck end’s impact force is slightly larger than the struck end.

The tank car was also instrumented with a shear strain gage bridge on the stub sill for measuring the vertical coupler force (Figure 7). Figure 33 shows the results of comparing longitudinal coupler force and vertical coupler force on the struck end of the car. The results show that vertical coupler force was much lower than longitudinal coupler force during the impact tests.

The results also show that the vertical force versus longitudinal force data was very scattered especially when steel friction draft gear was used. This could be because of the highly nonlinear nature of stick-slip behavior of steel friction gears. [Figure 33](#) shows that there was no clear relationship between longitudinal and vertical coupler forces during impact tests.

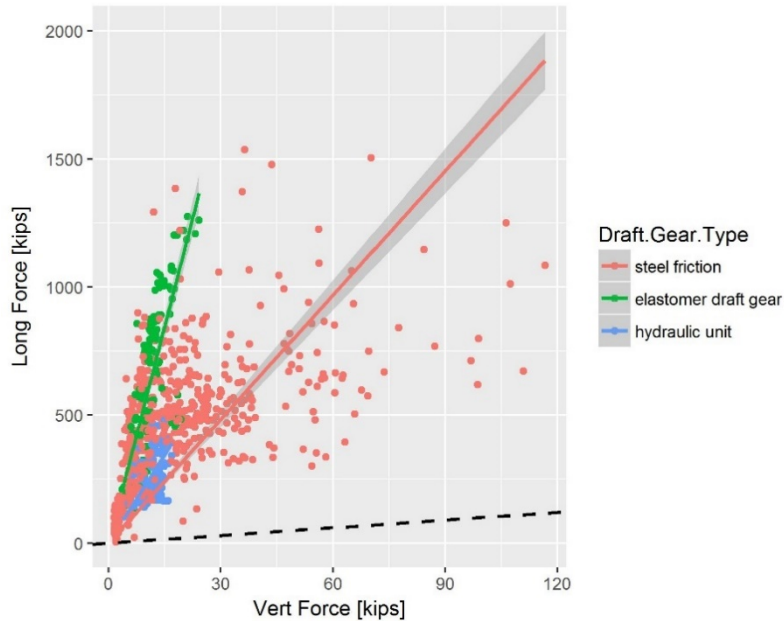


**Figure 33. Comparison of Longitudinal Coupler Force and Vertical Coupler Force on Struck End of Car**

### 3.4 Strain Gage Data Analysis

The tank car was instrumented with five sets of rosette strain gages placed at different locations around the stub sill that were identified as high stress locations. [Figure 8](#) through [Figure 12](#) illustrate the strain gages and their locations. Each rosette consisted of 3 uniaxial strain gages, resulting in 15 strain gage channels being recorded during impact testing.

The maximum strain during each impact test for each channel was obtained. [Figure 34](#) shows boxplots comparing the magnitude of each strain measured during the test program. Results show that the in-board strain gage experiences the highest strains. This agrees with the observation of frequent ruptures around in-board locations during tank car crashes. The lowest strains were observed near the shoulder pad.

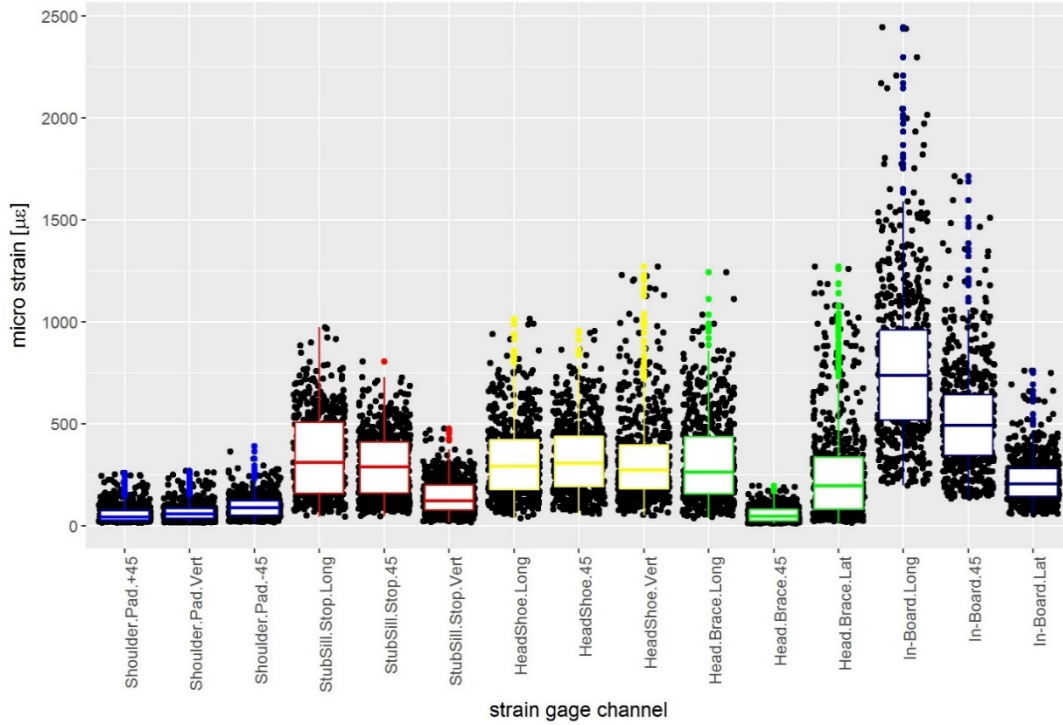


**Figure 34. Boxplot Comparison of Strain Magnitudes Throughout Test Program**

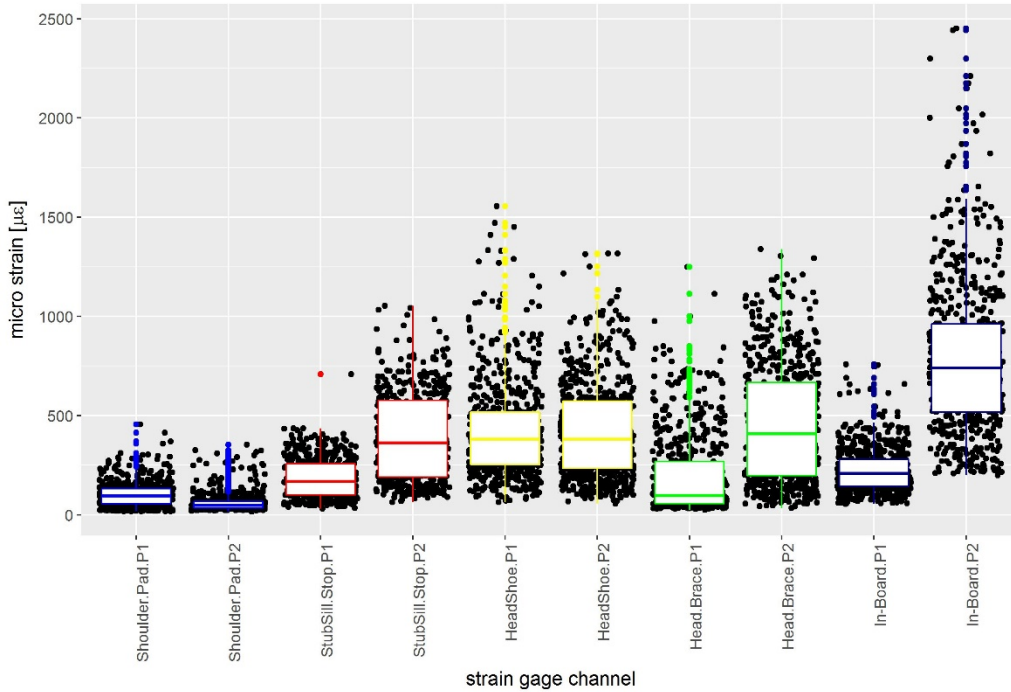
For each rosette set, the two principal strains are calculated from three strain readings as shown below:

$$\begin{cases} \varepsilon_{P1} = \frac{1}{2} \cdot (\varepsilon_1 + \varepsilon_3) + \frac{1}{2} \cdot \sqrt{(\varepsilon_1 - \varepsilon_3)^2 + (2 \cdot \varepsilon_2 - \varepsilon_1 - \varepsilon_3)^2} \\ \varepsilon_{P2} = \frac{1}{2} \cdot (\varepsilon_1 + \varepsilon_3) - \frac{1}{2} \cdot \sqrt{(\varepsilon_1 - \varepsilon_3)^2 + (2 \cdot \varepsilon_2 - \varepsilon_1 - \varepsilon_3)^2} \end{cases}$$

where  $\varepsilon_{P1}$  and  $\varepsilon_{P2}$  are the calculated principal strains and  $\varepsilon_1$ ,  $\varepsilon_2$ , and  $\varepsilon_3$  are the three strain readings for rosette set. The angle ( $\emptyset$ ) between  $\varepsilon_1$  axis and principal strain  $\varepsilon_{P1}$  is calculated as:

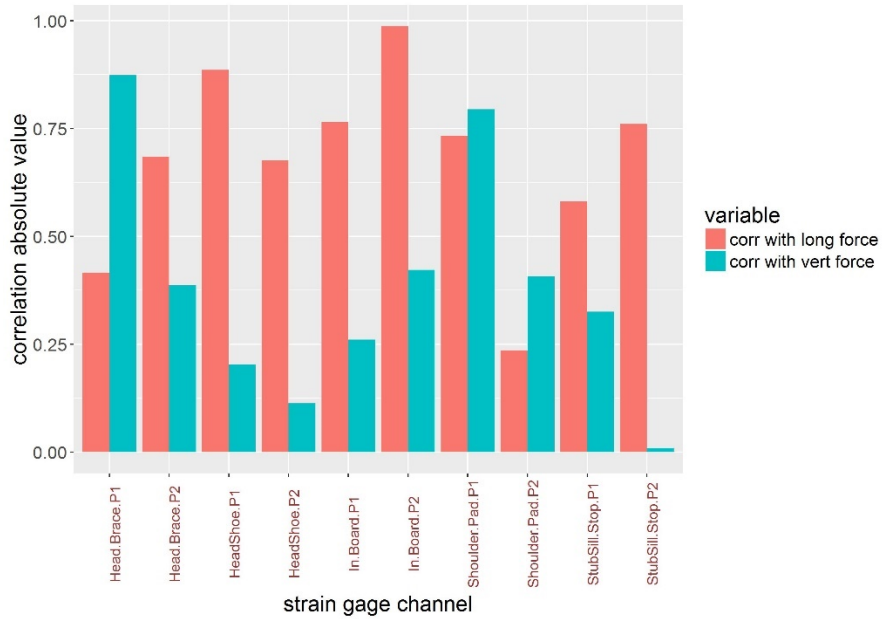
$$\tan 2\emptyset = \frac{2 \cdot \varepsilon_2 - \varepsilon_1 - \varepsilon_3}{\varepsilon_1 - \varepsilon_3}$$

Figure 35 shows the comparison of principal strains for different strain gage locations.



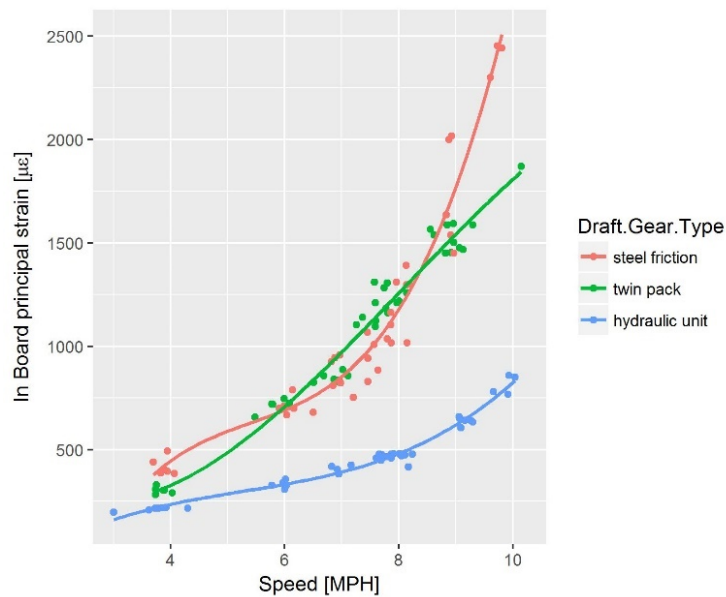
**Figure 35. Boxplot Comparison of Principal Strains Throughout Test Program at Different Locations on Test Car**

The railroad industry is interested in alternative approaches to the instrumented coupler for measuring coupling forces. The correlation between strain gage channels and longitudinal coupler force readings as well as vertical coupler force readings was studied. [Figure 36](#) shows the results of the correlation between strain gage channels and both vertical and longitudinal force channels. In-board strains appears to have the strongest correlation with longitudinal coupler force. The head brace principal strain appears to have the strongest correlation with vertical force readings.



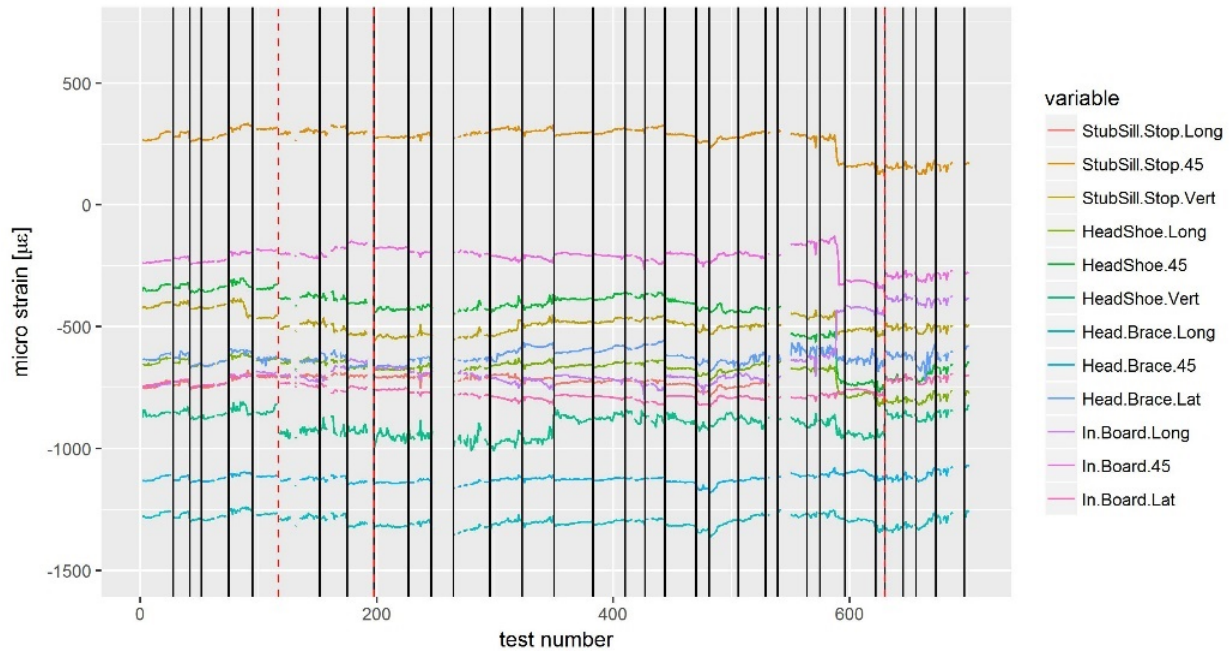
**Figure 36. Correlation Between Strains and Both Vertical and Longitudinal Coupler Forces**

Figure 37 shows the in-board principal strain versus coupling speed for different draft gear types with a full tank car and three hopper cars with brakes applied used as the anvil (Figure 29-right). There is a very similar trend for different draft gear types between longitudinal coupler force and in-board principal strain. This indicates that in-board strain measurements are a potential candidate for replacing instrumented couplers.



**Figure 37. In-Board Principal Strain versus Coupling Speed for Different Draft Gear Types, Full Tank Car and Three Hopper Cars with Brake on Used as Anvil**

The strain gage readings were assessed to see if there was any permanent shift in the strain readings. Strains were measured prior to and following each test with the tank car at rest. Figure 38 shows the permanent shift in strain readings for each channel during the time of the test program. Test Number 1 represents the beginning of the test program and Test Number 702 represents the last test of the program. Each solid black line indicates the first test of the day, meaning the car was parked outside one or more nights. Red dashed lines indicate water delivery dates as documented in Table 2. The results show that there is no apparent shift in the strain readings. However, there is a big jump in the strain readings around Test Number 590. The big jump might indicate an event of crack initiation and release of residual stresses in the car.



**Figure 38. Permanent Shift in Strain Readings During Test Program**

### 3.5 Acceleration Data Analysis

The tank car was instrumented with three accelerometers—two dual-axis accelerometers on the stub sill at each end of the car and one tri-axial accelerometer on the carbody—as shown in Figure 13 and Figure 14. The acceleration data were compared to longitudinal and vertical coupler forces to identify any possible correlations. Table 6 shows the correlation coefficient between acceleration channels and both vertical and longitudinal coupler forces. The results show that none of the acceleration channels had a strong correlation with vertical coupler force. However, longitudinal carbody acceleration had a strong correlation with longitudinal coupler force. Therefore, longitudinal carbody accelerations may be a potential candidate for replacement of longitudinal force measurements made by an instrumented coupler.

**Table 5. Correlation Coefficient Between Accelerations and Both Vertical and Longitudinal Coupler Forces**

Acceleration	Correlation with Longitudinal Coupler Force	Correlation with Vertical Coupler Force
Carbody Longitudinal	0.907	0.635
Carbody Vertical	0.702	0.564
Carbody Lateral	0.541	0.064
A-End Stub Sill Longitudinal	0.448	0.314
A-End Stub Sill Vertical	0.507	0.231
B-End Stub Sill Longitudinal	0.405	0.044
B-End Stub Sill Vertical	0.398	0.108

### 3.6 Impact Force versus Impulse

In the force data analysis, [Figure 27](#) showed that hammer configuration does not have much of an effect on the coupling force. To explain the physics behind why a full tank car with a weight more than three times that of an empty tank car resulted in the same coupling force for the same coupling speed, this section considers the transferred energy between coupling cars during impact.

The impulse was used as a measure of transferred energy between cars during impact. The impulse was calculated by integrating the impact force during the time period of the impact. The impulse, based on Newton’s second law, is equal to the change of momentum:

$$J = \int F dt = \Delta P = mv_2 - mv_1$$

where  $J$  is the impulse and  $\Delta P$  is the change of momentum during impact.

[Figure 39](#) shows the comparison of coupling force during impact for three impacting cars with different weights. The other coupling conditions (i.e., anvil configuration, draft gear type, and coupling speed) for three impact tests were the same. The coupling speed for all three tests were approximately 7 mph. [Table 7](#) shows the weight of impacting cars.

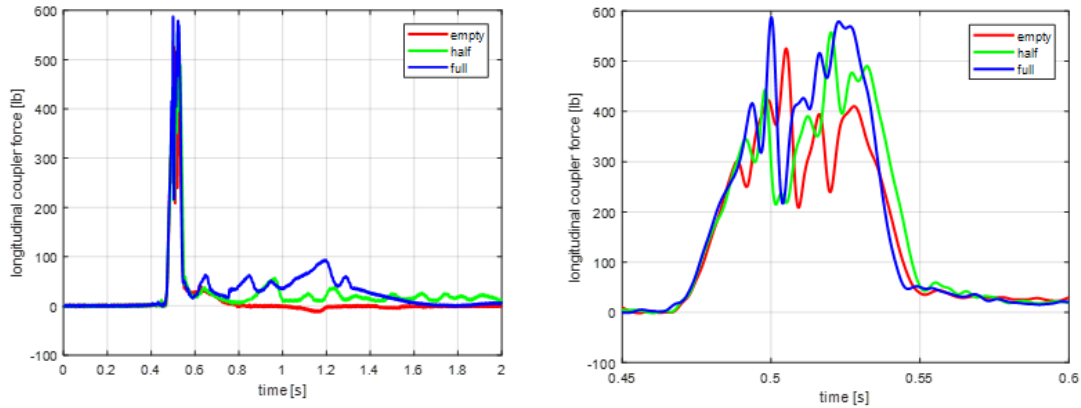


**Figure 39. Comparison of Coupling Force During Impact Empty, Half-Full and Full Tank Cars**

**Table 6. Comparison of Impact Force and Impulse (Area Under Force Curve) for Three Impact Tests with Different Weights of Hammer Cars**

<b>Hammer Car</b>	<b>Weight [kips]</b>	<b>Peak impact force [kips]</b>	<b>Impulse [kips-sec]</b>
Empty Tank Car	78.1	525	24.3
Half-Filled Tank Car	179.4	557	51.8
Full Tank Car	263.2	587	68.2

In [Figure 39](#), the left plot shows the coupling forces for a wider time range to capture the forces after the impact, whereas the right plot shows the same coupling forces during the impact time. [Table 7](#) shows the peak impact force calculated for the three impact tests. The results show that the force profile at impact looked very similar for different impacting weights with almost the same peak value.

However, the impulse is considerably different for different impacting weights. [Table 7](#) shows the impulse calculated for the three impact tests. The impulse was calculated as the area under the force curve. The impulse, which is a measure of transferred energy, accounted for the aftermath of the impact including water sloshing inside the filled tank car, causing a considerable difference between empty tank car's impulse and full tank car's impulse during impact. This showed that although the peak impact force for the three tests were similar, the impulse (i.e., transferred energy) were different while reflecting the weight of impacting cars.

### 3.7 Impulse Data Analysis

Much like force data analysis, impulse data was studied. The impulse was calculated by integrating the impact force during the time of the impact. [Figure 40](#) shows impulse data for different hammer configurations and a given anvil configuration. The anvil configuration is one hopper car with the brake on (left) and three hopper cars with the brake on (right). Tank cars of different weights were used to create different hammer configurations like [Figure 27](#). The results show that the weight of the hammer tank car had considerable effect on the impulse

(Figure 40), although the tank car's weight had limited effect on the peak impact force (Figure 27). This is in line with Newton's law since larger mass corresponds to larger momentum, thus, higher energy transfer.

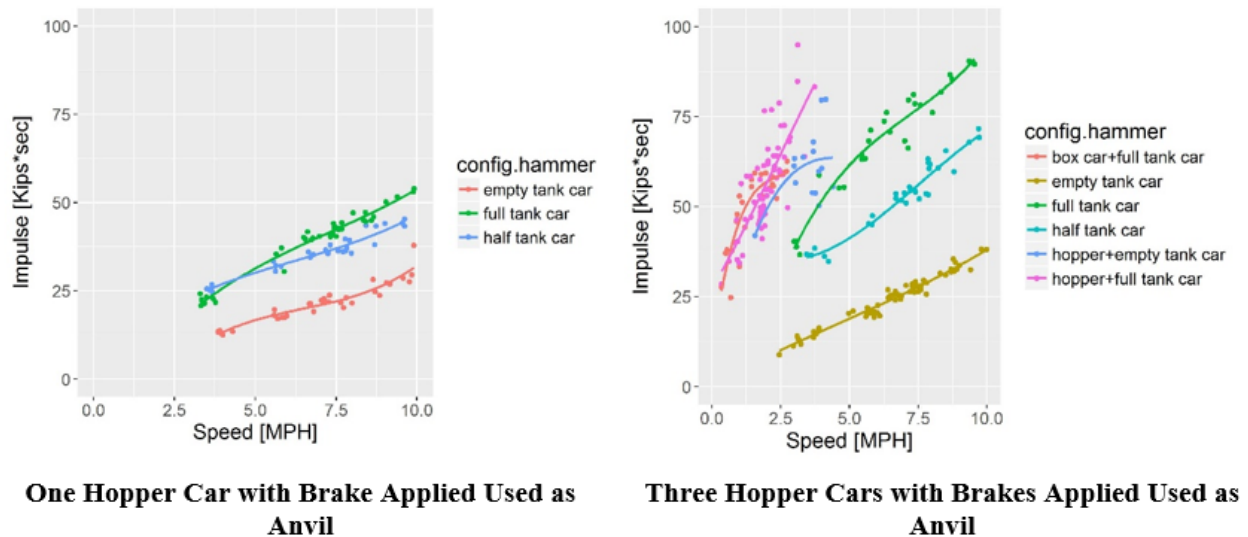
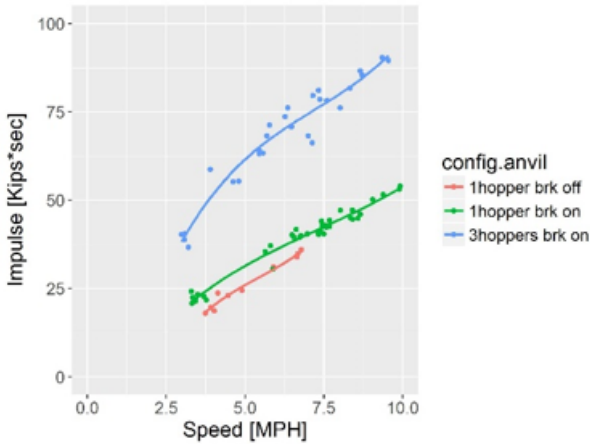
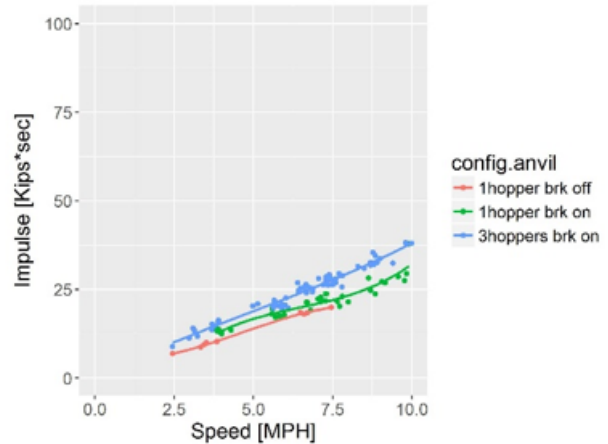


**Figure 40. Impulse Data Comparison for Various Hammer Configurations and Anvil Configurations with One and Three Hopper Cars with Brakes On**

Figure 41 shows impulse data for different anvil configurations and a given hammer configuration. The hammer car is a full tank car (left) and empty tank car (right). Various consist layouts were used for different anvil configurations. The results show that the anvil configurations, depending on the hammer configuration, had considerable effect on the impulse. A full tank car (Figure 41-left), unlike an empty tank car (Figure 41-right), striking different anvil configurations caused considerably different impulses during impact. This is in line with Newton's law since different anvil consists cause a different car momentum for a large mass hammer (full tank car) unlike a small mass hammer (empty tank car) after impact.



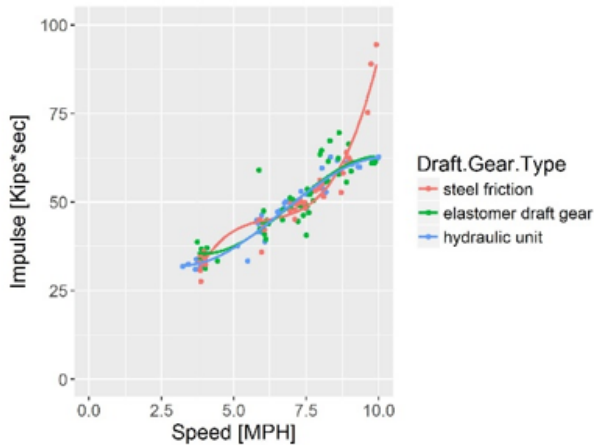
**Full Tank Car Used as Hammer**



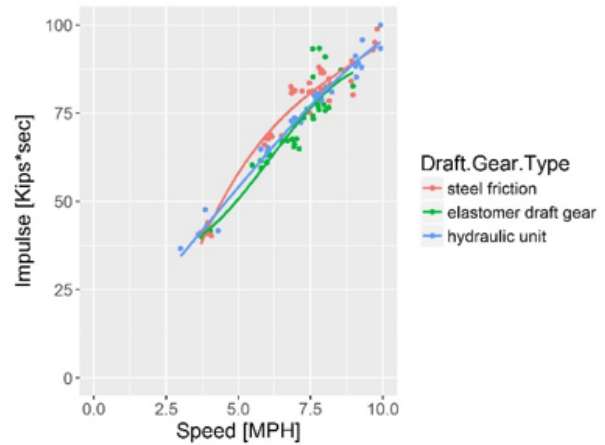
**Empty Tank Car Used as Hammer**

**Figure 41. Impulse Data Comparison for Different Anvil Configurations and Hammer Configurations Using Full and Empty Tank Cars**

Figure 42 shows impulse data for different end-of-car units for a given hammer and multiple anvil configurations. The anvil configuration is a full tank car with the brake on (left) and a full tank car plus three hopper cars (right). The results show that the end-of-car unit did not have any considerable effect on the impulse imparted to the anvil cars.



**Full Tank Car with Brake Applied Used as Anvil**



**Full Tank Car and Three Hopper Cars with Brakes Applied Used as Anvil**

**Figure 42. Impact Force Data Comparison for Different End-of-Car Units for Given Hammer and Anvil Configurations**

Unlike peak impact force, impulse is mainly affected by hammer and anvil configurations rather than draft gear type. According to physics, the transferred energy is equal to change of momentum at the impact. Therefore, the transferred energy is mainly affected by the mass of the impacting car as well as its speed before and after the impact.

## 4. Conclusion

---

A comprehensive test program focused on tank car impacts was conducted. Various coupling conditions were tested to characterize load environment at the impact. The following major conclusions were drawn from the data analysis:

- Results showed that coupling speed and end-of-car unit type have the most influence on the peak longitudinal impact force, whereas anvil and hammer consist configurations have limited effect on the peak impact force.
- Results showed that the end-of-car unit type has limited effect on the transferred energy between impacting cars, whereas hammer and anvil consist configurations have considerable effect on the transferred energy.
- Results showed that different end-of-car units perform differently in terms of impact force for different speed ranges. Hydraulic cushioning unit outperformed both steel friction and elastomer draft gears for all speed ranges. The elastomer draft gear performed better for lower coupling speed ranges compared to steel friction draft gears. Elastomer draft gear and hydraulic unit results were very consistent, but the force associated with the steel friction gear was more scattered.
- The instrumented coupler readings from both ends of the tank car showed that the non-struck end forces are comparable to struck end forces. This indicates that the impact force passes through the anvil consist, hence all the cars in the anvil consist experience the same impact force.
- The results showed that vertical coupler force was much lower than longitudinal coupler force during tests simulating hump yard operations. The results also showed that the vertical force versus longitudinal force data was very scattered especially for couplings involving steel friction gear.
- The results showed that in-board locations experience the highest strains, whereas the shoulder pad area experiences the lowest strain.
- The analysis of permanent shift in the strain readings revealed a big jump in the strain readings that might indicate an event of crack initiation and release of residual stresses in the car.

The load characterization results from this research will be combined with fatigue characteristics of stub sill material to design the yard operation scenarios. The limits on mass and speed combinations should be designed based on expected life of tank cars. This report serves as a steppingstone for such analysis with providing the extent of impact loading and energy transferred during yard operations, as well as the effect of different factors on the impact behavior.

## 5. References

---

Sundaram, N. (2014). [\*Force Environment Evaluation of Stub Sills on Tank Cars Using Autonomous Over-the-Road Testing of the Instrumented Tank Car\*](#). Technical Report, Report No. DOT/FRA/ORD-16/39. Federal Railroad Administration. Washington, DC: U.S. Department of Transportation.

## Abbreviations and Acronyms

---

ACRONYMS	EXPLANATION
R <sup>2</sup>	Coefficient of Determination
FRA	Federal Railroad Administration
HAZMAT	Hazardous Materials
RTV	Room Temperature Vulcanized *silicone rubber coatings*